American Journal of Science

CARBON CYCLE EVOLUTION BEFORE AND AFTER THE GREAT OXIDATION OF THE ATMOSPHERE

DON E. CANFIELD

ABSTRACT. The rock record of organic carbon abundance and its isotopic composition is consistent with the evolution of life more than 3800 million years ago (Ma). Despite this, there are very few insights as to the ecology of this ancient biosphere or to its level of activity. One possible insight, however, comes from the isotopic composition of inorganic and organic carbon in ancient rocks. This isotope record can be used, in principle, to determine the proportion of inorganic carbon entering the oceans that was buried in sediments as organic matter, and thus it helps constrain the activity level of the ancient biosphere. A quantitative analysis of this isotope record, however, requires that we understand how the Earth-surface carbon reservoir has evolved over time, as burial rates of organic matter in marine sediments depend on the input rates of carbon to the oceans. We must also know how organic matter is weathered as a function of atmospheric oxygen concentrations, thus indicating how much of the organic matter in sediments is newly formed or recycled. To explore these issues, a carbon cycle model is developed here that includes an evolving Earth-surface carbon reservoir as well as the oxygen dependency of the organic matter weathering in rocks. The model also allows for the release of CO_2 from organic matter during metamorphism and it contains a rock cycle with young and old reservoirs with appropriate transfer fluxes between them. The model shows that before the Great Oxidation Event (GOE) about 2400 Ma, only about 5 percent to 10 percent as much organic matter was buried into marine sediments as compared with today. Such low rates of organic matter burial would be consistent with a subdued marine biosphere. Such a subdued biosphere could possibly be consistent with primary production driven by anoxygenic photosynthesis coupled to an iron cycle. In association with, and in the aftermath of, the GOE, the biosphere likely increased its activity level by an order of magnitude. This large increase would have completely transformed the biology of the Earth and could have resulted from either the evolution and/or expansion of oxygen-producing cyanobacteria or a dramatic increase in the availability of nutrients to fuel oxygenic phototrophs.

Key words: carbon isotope, Archean, Proterozoic, GOE, Lomagundi, evolution, oxygen, cyanobacteria, carbon burial, carbon cycle, model, rock cycle

INTRODUCTION

The Hadean (4550–4000 Ma) and Archean (4000–2500 Ma) Eons represent, together, 44 percent of all Earth history. Little is known, however, of the Hadean environment as no rocks are available, and only mineral grains are preserved. An Hadean-aged zircon grain from 4100 Ma contains traces of disordered graphite with a $\delta^{13}C$ of −24 permil, consistent with organic matter production by organisms (Bell and others, 2015), and the oxygen isotopic composition of zircon grains from 4400 to 4300 Ma is

Department of Biology Nordcee and DIAS (Danish Institute for Advanced Studies), University of Southern Denmark, Campusvej 55, 5230 Odense M, Denmark
Corresponding author dec@biology.sdu.dk

consistent with the emergence of continental crust and of liquid oceans by that time (Mojzsis and others, 2001; Wilde and others, 2001).

Some early Archean sedimentary rocks from Isua, Greenland, contain layers of abundant graphite with $\delta^{13}C$ values as low as -20 permil (Rosing, 1999), consistent with a biological source, while kerogens from 3500 Ga hydrothermal dikes from the North Pole region, western Australia, have $\delta^{13}C$ values as low as -38 permil, consistent not only with life but also with methanotrophy in the hydrothermal system (Ueno and others, 2004). Indeed, fluid inclusions from these hydrothermal deposits contain methane with $\delta^{13}C$ values as low as -56 permil, consistent with the biological production of methane by methanogensis (Ueno and others, 2006). In addition, sedimentary rocks from the 3400 Ma Buck Reef Chert from South Africa contain organic matter in deep-water facies with $\delta^{13}C$ values of around -20 permil, and with values of -30 to -35 permil in shallow-water facies (Tice and Lowe, 2006b). These isotopic values are consistent with a biological origin for the organic matter, and perhaps also with multiple stages of biological processing in the shallow settings including methanogenesis and methanotrophy (Tice and Lowe, 2006b). The shallow settings also contained microbial mats that may have formed by photosynthetic organisms (Tice and Lowe, 2004), possibly anoxygenic phototrophs (Tice and Lowe, 2006a).

While these studies are consistent with a biological origin for organic matter production by early Archean times, and perhaps before, the history of photosynthetic oxygen production is both equivocal and indirect. For example, there is evidence for the oxidative weathering and mobilization of Cr and U from the 3000 Ma Nsuze paleosol from the Pongola Supergroup, South Africa (Crowe and others, 2013). Modeling of these results is consistent with levels of atmospheric oxygen at least 3×10^{-4} present atmospheric levels (PAL), concentrations high enough to seemingly require photosynthetic oxygen production (Crowe and others, 2013). There is also evidence for the oxidative cycling of trace metals in younger *ca.* 2600 to 2500 Ma Archean rocks (for example, Anbar and others, 2007; Wille and others, 2007), consistent with the presence of photosynthetic oxygen production. It is argued that these episodes of atmospheric oxygenation represent "whiffs" of atmospheric oxygen (Anbar and others, 2007) to levels elevated over a general baseline of $< 10^{-5}$ of PAL as constrained from the record of minor sulfur isotopes and its modeling (Farquhar and others, 2000; Pavlov and Kasting, 2002; Bekker and others, 2004; Zahnle and others, 2006; Farquhar and others, 2007).

Recent molecular clock estimates, however, suggest that cyanobacteria emerged in the late Archean Eon, with stem group cyanobacteria evolving some 2500 to 2800 Ma and with crown group diversification sometime between 2700 and 2000 Ma (Shih and others, 2017; Magnabosco and others, 2018). These estimates place the origin and diversification of cyanobacteria in approximate timing with a profound oxidation of the Earth's atmosphere that occurred around 2400 to 2300 Ma (Holland, 1994; Bekker and others, 2004; Farquhar and others, 2007), where atmospheric oxygen levels rose from low concentrations (Pavlov and Kasting, 2002) to concentrations that may have approached Phanerozoic Eon levels between 2350 and 2000 Ma (Bekker and Holland, 2012; Bachan and Kump, 2015). There is also a suggested link between the evolution of cyanobacteria and the rise of oxygen during the GOE (for example, Shih and others, 2017). If, however, cyanobacteria first emerged in the late Archean Eon, and in association with the GOE, then oxidants other than oxygen must have been responsible for the mobilization of trace metals in earlier Archean times (Martin and others, 2018), although it is not clear what these oxidants would have been.

Regardless of when cyanobacteria evolved, their impact on life and the environment would have been profound. Other than the obvious production of oxygen, leading to the evolution and expansion of aerobic organisms, cyanobacteria use water as

the electron donor. As water is abundant, the emergence of cyanobacteria likely elevated the activity level in the biosphere dramatically over what was possible with more dispersed electron donors like Fe^{2+}, H_2S and H_2 (for example, Canfield and others, 2006; Ward and Shih, 2019). In one estimate, an H_2-based biosphere would have been about 1 percent as active as today's marine biosphere, while a sulfur-based biosphere would have been 10 times less active than this. The most active biosphere would have been based on iron recycling, and such a biosphere may have been up to 10 percent as active as today's biosphere (Canfield and others, 2006).

In principle, the isotopic compositions of inorganic and organic carbon can be used to evaluate, at least broadly, the activity level of the ancient biosphere. This is because, in the most general terms, the isotopic composition of carbonate in seawater responds to the burial in sediments of isotopically distinct organic carbon. In this way, the proportion of the carbon entering the oceans and buried as organic matter can be evaluated from the isotopic compositions of organic and inorganic carbon in contemporaneous rocks. Thus, from a simple mass balance:

$$\delta^{13}C_{in} = \delta^{13}C_{org}f_{org} + \delta^{13}C_{IC}(1 - f_{org}) \tag{1}$$

where $\delta^{13}C_{in}$ is the isotopic composition of inorganic carbon entering the oceans, $\delta^{13}C_{IC}$ is the isotopic composition of inorganic carbon precipitated from the oceans as carbonate, $\delta^{13}C_{org}$ is the isotopic composition of organic matter removed to sediments, and f_{org} is the proportion of the total carbon removed from the oceans as organic matter. This expression can be rewritten such that:

$$f_{org} = (\delta^{13}C_{IC} - \delta^{13}C_{in})/(\delta^{13}C_{IC} - \delta^{13}C_{org}) \tag{2}$$

Thus, with a knowledge of $\delta^{13}C_{in}$, and independent measures of $\delta^{13}C_{org}$ and $\delta^{13}C_{IC}$, f_{org} can be calculated. We can explore how this works with a sample calculation relevant for early Archean times. Thus, if we consider the early Archean biosphere, an $\delta^{13}C_{org}$ of -20 ‰ to -30 ‰ seems to be a reasonable range as noted above. A $\delta^{13}C_{IC}$ of 0 ‰ is also reasonable value based on multiple analyses of early Archean carbonate rocks (Schidlowski and others, 1983; Krissansen-Totton and others, 2015) (more on the carbonate record below). If we use a $\delta^{13}C_{in}$ of -5 permil, the mantle value (Des Marais and others, 1992), a range of f_{org} values from 0.17 to 0.25 are calculated. This range in f_{org} is similar to previous determinations of f_{org} during early Archean times (Krissansen-Totton and others, 2015) and means that somewhere between 17 percent to 25 percent of the inorganic carbon entering the oceans would have been buried as organic carbon. It might be assumed that this high range of f_{org} values implies a very active early-Archean biosphere to produce the organic carbon, especially considering that the present-day f_{org} is around 0.2 (Hayes and others, 1999). Such an active biosphere might also suggest the presence of oxygen-producing cyanobacteria in the ecosystem.

This assessment, however, is made with an incomplete accounting of the ancient carbon cycle. For example, the weathering of organic matter is oxygen sensitive (Chang and Berner, 1999; Petsch and others, 2000; Bolton and others, 2006), and lower oxygen levels could impact the amount of organic carbon recycling (Daines and others, 2017). Furthermore, the carbon cycle has evolved through time (Hayes and Waldbauer, 2006), and any assessment of the activity level of the biosphere based on an evaluation of f_{org} depends also on the rate with which inorganic carbon is introduced to the oceans. Also, in discussing the activity level of the ancient biosphere, we must also consider how primary production might scale with organic matter burial.

Therefore, given these uncertainties, a model is presented here where the evolution of carbon cycle dynamics is evaluated in light of the evolution of the crustal inventory of sedimentary rocks, the crustal inventory of carbon and the evolution of atmospheric oxygen concentrations. Overall, organic carbon burial rates are constrained from the existing carbon isotope record, including the influence of changing oxygen levels of the weathering of organic carbon on land. This modeling effort joins other new models considering the long-term evolution of biogeochemical cycles in the context of an evolving carbon cycle (for example, Alcott and others, 2019) and bears some similarities to the carbon cycle model of Miyazaki and others (2018). Indeed, Miyazaki and others (2018) also consider how the influence of oxygen on organic matter cycling could have influenced the carbon isotope record after the GOE, but they do not focus on the evolution of carbon cycle and rates of carbon cycle processes as is done here.

The Model

The model developed here takes its inspiration from the idea that in the rock cycle, the newest-formed rocks recycle the fastest (Berner, 1987; Berner and Canfield, 1989). The model also has an evolving carbon cycle (Hayes and Waldbauer, 2006), and in addition, the influence of oxygen on the weathering rates of organic carbon is considered (for example, Daines and others, 2017; Miyazaki and others, 2018; Alcott and others, 2019). The model also tracks the carbon cycle through a stable carbon isotope mass balance. Each of these issues will be explored below.

An Evolving Rock Cycle

While the continents have grown from nothing at the time the Earth was first formed to what we have today, there are wildly different reconstructions of the history of continental growth (Cawood and others, 2013; Harrison, 2020). These different growth models encompass a variety of approaches and isotope systems aimed at understanding the timing over which continental crustal material was extracted from the mantle. A particular unknown in generating these models is the rate with which continental crustal material is recycled back into the mantle (Harrison, 2020). For this reason, isotope systems may be consistent with a range of continental growths histories depending on assumptions on the history of crustal recycling (Harrison, 2020). As a minimum constraint on the growth of the continental crust, Korenaga (2018) proposed a more or less linear trend in continental growth from the time of Earth formation to now, recognizing that more crustal recycling will lead to an earlier accumulation of the continental crust. Indeed, Rosas and Korenaga (2018) argue that the Sm-Nd isotope system is best explained by an early rapid growth of the crust accompanied by rapid early recycling in the mantle. In this model the present volume of continental crust was in place by 3800 Ma.

The Standard Model adopted here lies in between these extreme growth model estimates and is based on the analysis of Dhuime and others (2012), which, in turn, is based on the combined analysis of hafnium and oxygen isotopes in detrital zircons allowing a differentiation between recycled and new continental crust. In this model, continentals reached 63 percent of the present volume by 3000 Ma. The continental growth model of Dhuime and others (2012) is approximated by the equation:

$$\%\text{CV} = -4.97 \times 10^{-6}(\text{Ma})^2 + 6.25 \times 10^{-4}(\text{Ma}) + 100 \tag{3}$$

where CV represents the present-day mass of continental rocks. However, we also explore a Rapid Growth continental growth model where the present volume of continental crust was in place by 3800 Ma. This model is in line with the early estimate of Armstrong (1981) and similar to the model of Rosas and Korenaga (2018).

From here, we consider the growth of the sedimentary rock reservoir. A recent analysis of the Macrostrat database (https://macrostrat.org) suggests that sedimentary rocks of North America have increased as a proportion of total crustal rocks by about one order of magnitude through time (Husson and Peters, 2017). This increase includes an approximately 25 percent increase from the Archean into the Proterozoic Eons and a further increase by about a factor of 8 into the Phanerozoic Eon. It is not obvious how crystalline rocks for the Archean and Proterozoic Eons would have been subject to less weathering, erosion, and delivery into marine sediments compared to rocks of the Phanerozoic Eon. Indeed, pre-Phanerozoic rocks generally display chemical indices of weathering indicating weathering intensities that were compatible to, or even greater than, weathering intensities from Phanerozoic-aged rocks (for example, Condie and others, 2001; González-Álvarez and Kerrich, 2012), suggesting active weathering during pre-Phanerozoic times. Thus, it seems possible that the current distribution of sedimentary rock proportions over time reflects an overprint of preferential sedimentary rock recycling, particularly of young sedimentary rocks. Preferential recycling of young sedimentary rocks might be expected as after deposition, sedimentary rocks are often susceptible to rapid erosion and recycling due to sealevel changes and to tectonic and other processes encouraging coastal uplift (for example, Veizer and Jansen, 1985; Berner, 1987; McLennan, 1988). This idea of rapid sediment recycling will be explored in more detail below. It is also possible that massive loss of pre-Phanerozoic-aged sedimentary rock occurred during the Neoproterozoic-aged "great unconformity" (for example, Delucia and others, 2017).

Thus, it is assumed here that the clastic sedimentary rock reservoir grew in proportion with the crustal reservoir. However, as we explore different and widely ranging crustal growth models, we also explore a reasonable range in the evolution of the sedimentary rock reservoir. We note that the evolution of the sedimentary rock reservoir, and not the evolution of the total crustal rock reservoir, is the primary input to the model. We do not, however, explore the proposal of Husson and Peters (2017) that the sedimentary rock reservoir was small during pre-Phanerozoic times, increasing by nearly an order of magnitude across the Proterozoic-Phanerozoic boundary. In all modeling scenarios, the carbonate rock reservoir grows as carbonates are precipitated from seawater as outlined below.

The rock cycle modeled here operates as envisioned for the Phanerozoic Eon (Berner, 1987; Berner and Canfield, 1989), where rocks are proportioned into a young reservoir subject to relatively rapid weathering, and an old reservoir subject to relatively slow weathering, with a transfer (aging) between the young and the old reservoirs (fig. 1). The young reservoir represents rocks more recently extracted from the oceans, while the old reservoir might be viewed as rocks in continental interiors and less subject to weathering (Berner, 1987; Berner and Canfield, 1989). While geologically reasonable, the partitioning of rocks into young and old reservoirs was initially introduced to buffer towards excessive swings in geochemical properties like atmosphere oxygen over time in models (Berner, 1987; Berner and Canfield, 1989). The current model does not explicitly contain an oxygen budget, but the young and old reservoir concept has been preserved.

The relative proportions of continental rock reservoirs, as well as the reservoir of modern marine sediments, are established here based on estimates for their volumes in Phanerozoic-aged rocks and sediments (table 1). As noted above, in the present model, all rock and sediment reservoirs retain these proportions as the continental reservoir of rocks grows through time. Thus, in the Standard Model, the mass of the various rock reservoirs over time, including the mass of marine sediments, become the modern mass of these reservoirs multiplied by CV (divided by 100) as given in Equation 1 and presented in figure 2A. In the Rapid Growth model, the sedimentary
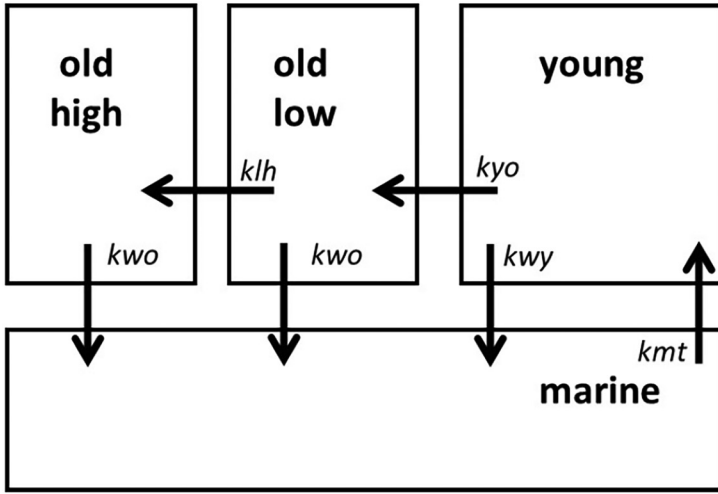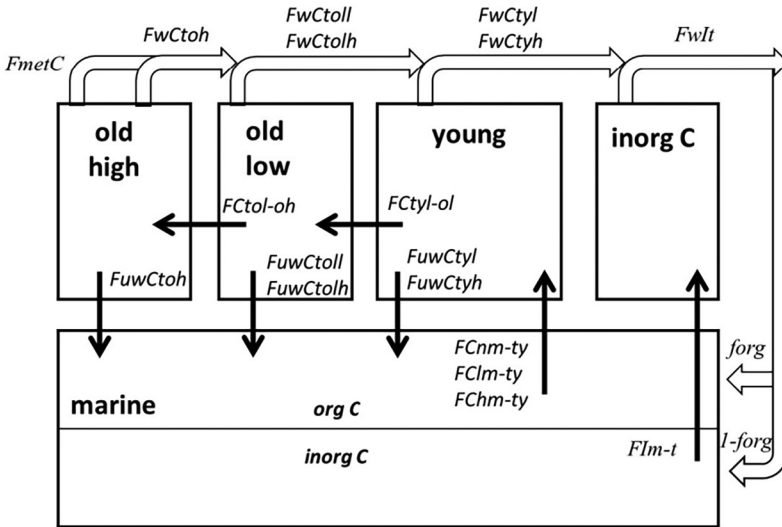
Fig. 1. Cartoons showing the evolution of the rock cycle and the carbon cycle as developed in this model. (A) The rock cycle is shown, with the rate constants "*k*" indicating the fluxes between the different compartments of the cycle. (B) Evolution of the carbon cycle with fluxes between different compartments show n. See table 2 for definitions and the text for details.

rock reservoir grows linearly from 4500 Ma to 3800 Ma to its present mass, and it remains constant from this time forward (fig. 2A).

Note that while the mass of deep-sea sediments is included in table 1, these sediments will not be considered explicitly in the calculations that follow as most of this sediment becomes subducted (Hay and others, 1988) with little trace in the terrestrial

TABLE 1
Mass of sediments and sedimentary rocks

setting	Total mass[a] x10²¹ g	Carbonate-free mass[b] x10²¹ g
Terrestrial		
Cratonic[1]	346	285
Geosyncline Precambrian to Paleozoic	524	419
Geosyncline Mesozoic to Cenozoic	503	402
total	1383	1106
Marine		
Passive margin	205	156
Active margin	41	31
Slope and rise	607	462
Deep-sea	249	129
total	1102	778 (649)[c]

[a]data from Southam and Hay (1981).

[b]assuming 20% calcium carbonate for terrestrial rocks after Holser and others (1988), 23.8% calcium carbonate for continental margin sediments calculated from an average inorganic carbon content of 2.86 wt% from Southam and Hay (1981), and 52% calcium carbonate for deep-sea sediments calculated from an average inorganic carbon content of 6.2 wt% from Holser and others (1988).

[c]not including deep-sea sediments.

record of sedimentary rocks. However, deep-sea processes as they relate to aspects of the carbon cycle will be considered implicitly as described below. Table 2 provides definitions of all the reservoirs, fluxes and other terms used in the modeling.

The rate constants, *kwy* and *kwo*, for rock weathering were determined for 2 scenarios as outlined by Berner (1987). In one scenario, the ratio between the weathering rates of the young and old rock reservoirs (*kwy/kwo*) is 4/1 and in the other scenario, the ratio is 9/1. Individual *k* values were determined assuming these different ratios and a total modern sediment flux to the oceans of 1.3×10^{16} g y^{-1} (Berner, 1987). Other estimates for the flux of sediment to the ocean include a total denudation rate estimate of 1.5×10^{16} g y^{-1} (Wittmann and others, 2020) and a total modern sediment discharge rate of 1.9×10^{16} g y^{-1} (Milliman and Farnsworth, 2013). The somewhat lower flux estimate used here (1.3×10^{16} g y^{-1}) is retained recognizing that modern river discharge may be somewhat higher than the long-term average due to the influence Pleistocene glaciation on erosion and sediment transport to the ocean (Herman and others, 2013). The basic equation for rock weathering is:

$$kwy * Mty + kwo * Mto = 1.3 \times 10^{16} \text{g y}^{-1} \qquad (4)$$

where *Mty* is the mass of the young terrestrial reservoir, *Mto* is the mass of the old terrestrial reservoir, and in addition, *kwy* = 4*kwo* or *kwy* = 9*kwo*. The *k* values are shown in table 3. After this, the rate constants associated with the transfer from the young to
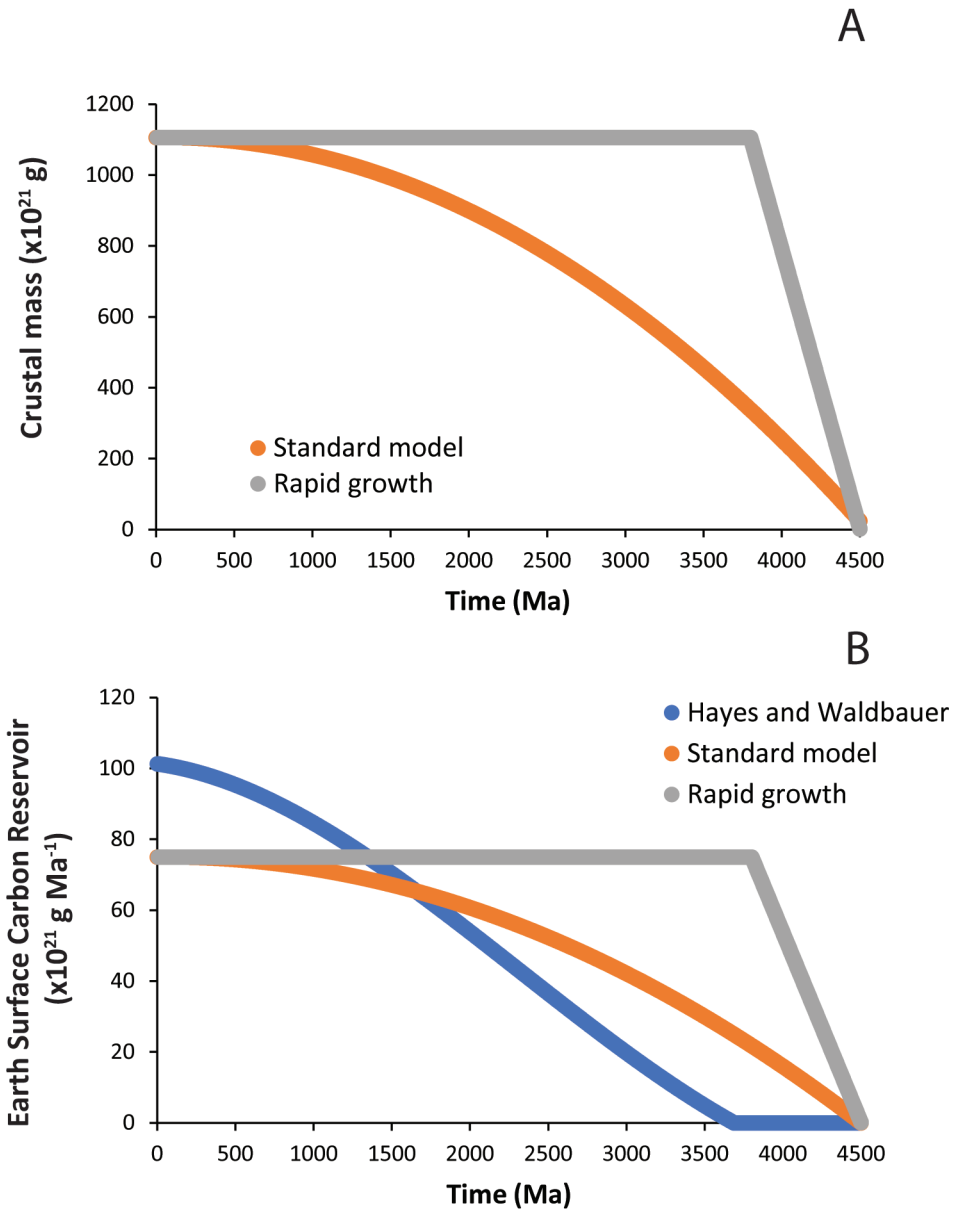
A

B

Fig. 2. Plots showing the evolution of the continental crust and carbon cycle in the current model. (A) Accumulation of continental crust through time from the both the Standard and Rapid Growth models. (B) The evolution of the Earth-surface carbon reservoir for 3 different models including the Standard Model and the Rapid Growth models of the current contribution and the results of a previous model proposed by Hayes and Waldbauer (Hayes and Waldbauer, 2006).

the old reservoir, kyo, are calculated. The rate constants are calculated to replace the mass of rock lost in the old reservoir by weathering, and the values are provided in table 3. In a subsequent study Berner and Canfield (1989) favored a value for a kwy/kwo of 4/1 yielding a transfer time ($1/kyo$) between the young reservoir and old reservoirs of about 100 million years. With a kwy/kwo of 9/1, the transfer time ($1/kyo$) between

TABLE 2

Terms and definitions

Term	Definition
Mty	mass of young terrestrial rock
Mtol	mass of old terrestrial rocks low grade
Mtoh	mass of old terrestrial rocks high grade
MIt	mass of terrestrial inorganic carbon pool
Mm	mass of marine sediment (carbonate free)
Ctyl	percent organic carbon in young low-grade pool
Cml	percent organic carbon in young high-grade pool
Cmh	percent high grade organic carbon in marine sediment
Cmn	percent new organic carbon in marine sediments
MIm	mass of marine inorganic carbon pool
Ctoll	percent low grade organic carbon in low grade terrestrial pool
Ctolh	percent of high-grade organic carbon in low grade terrestrial pool
CTotm	percent total organic carbon in marine sediments
Im	percent inorganic carbon in marine sediments
MCtyl	mass organic carbon in young low-grade pool
MCtyh	mass organic carbon in young high-grade pool
MCtohl	mass high grade organic carbon in old low-grade pool
MCtoll	mass low grade organic carbon in old low-grade pool
MCtoh	mass organic carbon in old high-grade pool
MCml	mass low organic grade carbon in marine sediments
MCmh	mass high grade carbon in marine sediment
MCmn	mass new carbon in marine sediments
Mm	mass of marine sediment
FCnet	net flux of CO_2 from the mantle
FwCtyl	weathering flux of organic carbon from young low-grade pool
FwCtyh	weathering flux of organic carbon from young high-grade pool
FwIt	weathering flux of inorganic carbon pool
FwCtoll	weathering flux of low-grade organic carbon from old low-grade pool
FwCtolh	weathering flux of high-grade organic matter from old low-grade pool
FwCtoh	weathering flux of organic carbon from old high-grade pool
FuwCtyl	flux of unweathered low-grade organic carbon from young low-grade pool
FuwCtyh	flux of unweathered high-grade organic carbon from young high-grade pool
FuwCtoll	flux of unweathered low-grade organic carbon from old low-grade pool
FuwCtolh	flux of unweathered high-grade organic matter from old low-grade pool
FuwCtoh	flux of unweathered high-grade organic carbon from old high-grade pool
FCtyl-ol	flux of low-grade organic carbon from young low-grade pool to old low-grade pool
FCtyh-ol	flux of high-grade organic carbon from young low-grade pool to old low-grade pool
FCtoll-oh	flux of low-grade organic carbon in old low-grade pool to high-grade pool
Ctolh-oh	flux of high-grade organic carbon in old low-grade pool transferred to high-grade pool during metamorphism
FmetC	flux of CO_2 released as low-grade organic carbon is metamorphosed to high-grade organic carbon
FCnm-ty	flux of new organic carbon from the marine to the terrestrial young reservoir
FClm-ty	flux of low-grade organic matter from marine to terrestrial young reservoir
FChm-ty	Flux of high-grade organic matter from marine to terrestrial young reservoir
FIm-t	Flux of inorganic carbon from marine to terrestrial young reservoir
FIt-m	total flux of DIC to oceans
Fsed	total flux of sediment to the oceans
MetaM	proportion of metamorphosed organic carbon returned to Earth surface as CO_2
delmantle	$\delta^{13}C$ of mantle CO_2
delSW	$\delta^{13}C$ of seawater
delBCmn	$\delta^{13}C$ of new carbon buried in marine sediments
delCmn	$\delta^{13}C$ of new organic carbon in marine sediments
delCml	$\delta^{13}C$ of low-grade organic carbon in marine sediments
delCmh	$\delta^{13}C$ of high-grade organic carbon in marine sediments
delCtyl	$\delta^{13}C$ of low-grade organic carbon in young terrestrial reservoir
delCtyh	$\delta^{13}C$ of high-grade organic carbon in young terrestrial reservoir
delCtoll	$\delta^{13}C$ of low-grade organic carbon in old low-grade terrestrial reservoir
delCtolh	$\delta^{13}C$ of high-grade organic carbon in old low-grade terrestrial reservoir
delCtohh	$\delta^{13}C$ of high-grade organic carbon in old high-grade terrestrial reservoir
delFItm	$\delta^{13}C$ of inorganic carbon flux from the terrestrial to the marine environment
PAL	fraction of present atmospheric level
Km	half saturation constant for organic matter weathering
Forg	fraction total carbon buried as organic carbon
Kwy	weathering constant for young rocks
Kwo	weathering constant for old rocks
Kwi	weathering constant for carbonate rocks
Kmt	transfer constant from marine to terrestrial
Klh	transfer constant from low-grade to high-grade terrestrial reservoir
Kyo	transfer constant from young to old terrestrial reservoir

Rate constants

	Rate constant my^{-1}
kwy=4kwo	
kwy	22.5×10^{-3}
kwo	5.62×10^{-3}
kyo	9.84×10^{-3}
klh	5.62×10^{-3}
kwy=9kwo	
kwy	27×10^{-3}
kwo	3.0×10^{-3}
kyo	5.26×10^{-3}
klh	3.0×10^{-3}
kwi	13×10^{-3}
kmt	2.0×10^{-3}

the young and old reservoirs is much longer at about 200 million years. The shorter transfer time with a *kwy/kwo* of 4/1 allows for faster response in terrestrial rocks to changes ultimately coming, in the present model, from changes in the carbon cycle of the oceans and the oxygen content of the atmosphere. In the modeling performed here, both values for *kwy/kwo* were explored with no substantive difference in model outcomes and conclusions. Therefore, in all subsequent modeling, a *kwy/kwo* of 4/1 will be used.

Marine sediments are the source of continental sedimentary rocks through sea-level change, uplift and other tectonic processes such as continental collision. It is assumed that the marine reservoir of sediments (carbonate-free and excluding deep-sea sediments) replaces the terrestrial rocks lost by weathering. Replacing these rocks yields a rate constant for the transfer from marine sediments to the terrestrial rock reservoir, *kmt*, of 0.02 Ma^{-1}. The reservoir of carbonate rocks also represents a substantial part of the rock record. The dynamics of the inorganic carbon cycle is dealt with separately and will be discussed in more detail when describing carbon cycle modeling.

Also introduced here is the idea that metamorphism will influence the carbon cycle. The carbon cycle, including the influence of metamorphism, will be dealt with in more detail below. But, in the context of the rock cycle as modeled here, metamorphism influences rocks of the "old" terrestrial reservoir. We are aware of no compilations of the distribution of metamorphic rocks through geologic time, but in the absence of this, it is assumed that 50 percent of the old rock reservoir is comprised of metamorphic rocks of high degrees of thermal maturity. In the context of the carbon cycle as discussed below, this would translate to upper greenschist grade metamorphic rocks heated to over 400 °C where graphite begins to form (Buseck and Huang, 1985) and where the metamorphic loss of carbon becomes important (Raiswell and Berner, 1987). To model the formation of metamorphic rocks, we assume that the mass of the old terrestrial high maturity reservoir (*Mtoh*) removed by weathering (equivalent to one half of the total mass of the terrestrial old reservoir, *Mto*) is replaced by metamorphic transformation from the old terrestrial low-maturity reservoir (*Mtol*). With the

TABLE 4

Distribution of carbon in Earth surface reservoirs

setting	Organic carbon $x10^{18}$ moles	Inorganic carbon $x10^{18}$ moles	Grand total
Terrestrial			
Cratonic	149	802	
Geosynclines	455	1971	
Marine			
Shelf/slope	350	200	
Deep-sea	63	1267	
Total (moles)	1014	5246	$6260x10^{18}$
Total (grams)	$12.2x10^{21}$	$63x10^{21}$	$75.2x10^{21}$

[a]Data from Holser and others (1988).

distribution of reservoir masses as shown in table 1, and as discussed above, the rate constants describing the transformation from the low maturity to high maturity terrestrial reservoir, *kl-h* are given in table 3 for both *kwy/kwo* = 4 and *kwy/kwo* = 9.

An Evolving Carbon Cycle

We begin with an inventory of the carbon reservoirs on the modern Earth (table 4). These values are taken from Holser and others (1988), yielding a total (both organic carbon and inorganic carbon) carbon inventory of 75×10^{21} g. In the carbon cycle modeling of Hayes and Waldbauer (2006), a total carbon inventory of 102×10^{21} g was assumed. This value was taken from Wilkinson and Walker (1989), who calculated carbon abundances from a number of sources, but for terrestrial carbon, relied on the volumes of various rock types through time as presented in Ronov and others (1980), with assumptions of porosity and carbonate contents for each rock type. However, separately, but using the same data, Ronov (1976) directly calculated the carbon inventory of terrestrial rocks at 61.4×10^{21} based on an estimate of total terrestrial rock mass of 1598×10^{21} g. The rock/carbon cycle developed here is based on the estimates of total rock mass from Southam and Hay (1981), with a somewhat lower estimate of 1383×10^{21} g (table 1). If Ronov's terrestrial carbon inventory is scaled to the terrestrial rock mass of Southam and Hay (1981), a carbon inventory of 53×10^{21} g is obtained. If this value is added to the carbon inventory of marine sediments (22.6×10^{21} g, table 1), the total carbon inventory becomes 75.6×10^{21} g, nearly identical to the value we use, and thus consistent with the available literature.

Taking inspiration from previous models (for example, Sleep and Zahnle, 2001; Hayes and Waldbauer, 2006), the carbon reservoir evolves through Earth history to its present inventory. The model developed here follows in the spirit of Hayes and Waldbauer (2006), who make the reasonable argument that the surface inventory of carbon could only grow as continents themselves grew in volume. Therefore, it is assumed here that the Earth-surface carbon reservoir accumulated in cadence with continental growth for each of the continental growth models explored here. In these cases, the carbon inventory at any time is the product of the current inventory and Equation 3 (divided by 100), expressing the percent of the current continental crustal

volume over time (fig. 1B). In addition, we also explore directly the carbon growth model of Hayes and Waldbauer (2006), and finally, we explore cross models where the carbon inventory history from the Standard model is combined with the sediment inventory of the Rapid Growth crustal model, and vice versa.

In reality, the carbon that accumulates in the surface environment is the net result of degassing of CO_2 from the mantle and the removal of marine carbon back into the mantle through both the subduction of carbon in sediments and the weathering (carbonatization) of mid-ocean ridge basalts as seawater circulates through these rocks. Such an approach was taken by Hayes and Waldbauer (2006) to model the accumulation of the carbon reservoir, and these steps are implicit in the approach taken here as we consider the net accumulation of carbon into the Earth surface reservoir.

After carbon is introduced to the Earth surface, the carbon cycle evolves dynamically. The model develops in time steps of 1 million years, and in the first step, CO_2 enters the surface environment from the mantle. This flux, *FCnet*, is deposited into marine sediments, as either new organic carbon, *FCmn* (flux of organic carbon into the new marine reservoir) or inorganic carbon, *FIm* (flux of inorganic carbon into marine reservoir) depending on the *forg*, which defines the proportion of the total carbon buried in marine sediments as organic carbon as described above.

$$FCmn = FCnet * forg \qquad (6)$$

$$FIm = FCnet - FCmn \qquad (7)$$

In the subsequent steps, a portion of the marine carbon reservoir, including both organic carbon and inorganic carbon, is transferred to the terrestrial young reservoir as low-grade organic matter depending on the transfer kinetics as described above. This organic carbon becomes subject to weathering and to transfer to the other terrestrial reservoirs as described above and as shown in figure 1. We can follow, for example, evolution of the young terrestrial low-grade organic carbon pool, *MCtyl*:

$$MCytl_{i+1} = MCtyl_i + FCnm\text{-}ty + FClm\text{-}ty - FwCtyl - FuwCtyl - FCtyl\text{-}ol \qquad (8)$$

where $MCytl_{i+1}$ represents the mass of the young terrestrial low-grade organic carbon reservoir at time $i + 1$, and $MCtyl_i$ represents the mass of this reservoir at time i. Other parameters include *FCnm-ty*, the flux of new organic carbon from the marine to the terrestrial young reservoir, *FClm-ty*, the flux of low-grade organic matter from the marine to the terrestrial young reservoir *FwCtyl*, the weathering flux of organic carbon from the young low-grade pool, *FuwCtyl*, the flux of unweathered low-grade organic carbon from the young low-grade pool and *FCtyl-ol*, the flux of low-grade organic carbon from the young low-grade pool to the old low-grade pool (see table 2 for definitions). The fluxes and reservoir sizes of the carbon cycle as developed here are fully described in the interactive model presented in the supplemental Excel sheet (http://earth.geology.yale.edu/%7eajs/SupplementaryData/2021/Canfield).   Note that model does not contain an atmospheric reservoir for CO_2.

After the terrestrial reservoir accumulates, and after a few initial time steps, the flux of inorganic carbon to the marine realm, *FItm*, includes, in addition to outgassing from the mantle, weathering from the terrestrial organic and inorganic pools and the metamorphic release of CO_2:

$$FItm = FCnet + FwIt + FwCtyl + FwCtyh + FwCtoll + FwCtolh + FwCtoh + FmetC \qquad (9)$$

where *FCnet* is the net flux of CO_2 from the mantle, *FwIt,* the weathering flux from the inorganic carbon pool, *FwCtyl,* the weathering flux of organic carbon from the young low-grade pool, *FwCtyh,* the weathering flux of carbon from the young high-grade pool, *FwCtoll,* the weathering flux of low-grade organic carbon from the old low-grade pool, *FwCtolh,* the weathering flux of high-grade organic matter from the old low-grade pool, *FwCtoh,* weathering flux of high-grade organic matter from the old low-grade pool and *FmetC* is the flux of CO_2 released as low-grade organic carbon is metamorphosed to high-grade organic carbon . With these fluxes, an evolving pool of inorganic carbon becomes available to fuel primary production in the oceans, and after the first initial time step (Equation 6), the burial of new organic matter in the oceans, *FCmn,* becomes:

$$FCmn = FItm*forg \tag{10}$$

and the burial of inorganic carbon in the oceans, *FIm,* becomes:

$$FIm = FItm - FCmn \tag{11}$$

Inorganic carbon on land forms its own terrestrial reservoir. This reservoir accumulates based on the balance between addition from the marine environment, *FImt,* and weathering, *FwIt*:

$$MIt_{i+1} = MIt_i + FImt - FwIt \tag{12}$$

and:

$$FwIt = kwi*MIt \tag{13}$$

The rate constant associated with weathering of the inorganic carbonate pool, *kwi*, is set at 0.013 Ma^{-1}. This value is 1.5 times the weathering rate of terrestrial rocks (including both the young and old terrestrial sedimentary rock reservoirs when taken together) as estimated by Mackenzie and Morse (1992). The modeling of the inorganic carbon pool is simpler than for organic carbon as there is no known relationship between inorganic carbon weatherability and oxygen concentration (as there is for organic matter as explored below), and we do not differentiate carbonate weatherability based on thermal maturity.

Returning to the organic carbon pool on land, a portion of organic carbon in the young terrestrial reservoir, *FCtyl,* will be transferred to the old terrestrial reservoir, *FCtol,* depending on the transfer kinetics:

$$FCtyl\text{-}ol = kyo * MCtyl \tag{14}$$

This organic matter is still considered to be of low thermal maturity. However, a portion of this low-maturity organic carbon in the old rock pool will be converted by metamorphism into high-maturity organic carbon, based on the flux *FCtoll-oh*:

$$FCtoll\text{-}oh = klh * MCtoll \tag{15}$$

During this metamorphic transformation, some amount of the organic carbon, *FmetC* (as noted above) will be oxidized and returned back to the Earth surface as CO_2:

$$FmetC = FCtoll\text{-}oh * MetaM \qquad (16)$$

where *MetaM* is that fraction of organic carbon undergoing metamorphism that is released as CO_2.

Indeed, the thermal heating and metamorphism of organic matter will lead to gaseous carbon products including both CO_2 and methane (CH_4) (Tissot and Welte, 1984). In presence of oxygen, the methane produced and liberated to the atmosphere will be rapidly (years) photolytically oxidized to CO_2, but in the absence of oxygen, the methane will be oxidized to hydrocarbons of intermediate oxidation levels that can polymerize and condense back to the Earth surface (Kasting and others, 1983), in essence returning organic matter to the surface reservoir. The present model will not track methane and thus will not account for potential differences in the methane cycle in the presence and absence of oxygen. However, *MetaM* is a free parameter, and different values will be explored that can accommodate different fates of the gaseous carbon products of metamorphism, as well as different overall amounts of carbon release during metamorphism. In the Standard Model a *MetaM* of 0.5 is adopted. This value is compatible with organic matter loss during both contact and regional metamorphism (for example, Clayton and Bostick, 1986; Raiswell and Berner, 1987; Agirrezabala and others, 2014).

Following Bolton and others (2006), the weathering of the terrestrial organic matter pools is oxygen-dependent following Michaelis-Menten kinetics. For example, the weathering flux of organic carbon in the low-maturity young reservoir, *FwCtyl* (gC Ma^{-1}) is expressed as:

$$FwCtyl = kwy * MCty * Rmaxl * \big(PAL/(PAL+km)\big) \qquad (17)$$

where, in addition to the terms already defined, *Rmaxl* (although unitless) represents the maximum oxidation rate of low-maturity organic matter (*Rmaxh* is the equivalent expression for high-maturity organic matter), *PAL* is the fraction of the present atmospheric oxygen level, and *km* is the half-saturation constant with respect to weathering. The organic matter that is unoxidized during rock weathering is transferred to ocean sediments as detritus carrying the same designation as it had on land. As an example, the flux of unweathered organic carbon in the low-maturity young reservoir to marine sediments, *FuwCtyl*, is given as:

$$FuwCtyl = kwy * MCty - FwCtyl \qquad (18)$$

To summarize, marine sediments accumulate detrital organic carbon from land, but also new organic carbon fueled by marine primary production. As noted above, the inorganic carbon available to fuel this primary production (*FItm*) includes degassing from the mantle, the oxidative weathering of organic carbon and the weathering of inorganic carbon on land, as well as the metamorphic release of CO_2. Thus, a mix of newly formed recycled detrital organic matter of various degrees of maturity are transported to the terrestrial young reservoir based on the kinetics of the formation of these rocks from marine sediments. In subsequent time steps, these processes continue as both continental land mass and the Earth-surface carbon reservoir accumulate and as dynamics change including variable atmospheric oxygen concentrations and changes in *forg*.

Oxygen-Dependent Organic Matter Oxidation

Field studies provide some insight into the weatherability of organic carbon and show, for example, that organic carbon in shales is oxidized much more readily than pyrite (Petsch and others, 2000; Petsch, 2014). Studies from both rivers and marine

sediments, however, show that the oxidation of rock-hosted "petrographic" organic carbon is not necessarily complete during weathering, and even today, with high atmospheric oxygen concentrations, some petrographic carbon is recycled through rivers and into marine sediments (Dickens and others, 2004a; Dickens and others, 2004b; Galy and others, 2008; Galy and others, 2015; Li and others, 2015; Bao and others, 2019, Blattmann and others, 2019).

Recycled petrographic carbon includes both graphite and kerogen, and the concentrations of recycled graphitic carbon have been determined in modern marine sediments in a few cases. Indeed, values of 0.031 wt% to 0.09 wt% have been determined for Washington shelf sediment (Dickens and others, 2004a; Haberstroh and others, 2006), with values of 0.016 wt% for sediments off the Mexican margin, 0.012 wt% for sediments of the Equatorial Pacific (Haberstroh and others, 2006) and 0.01 to 0.11 wt% for sediments of the Gulf of Cádiz (Spain) (Sánchez-García and others, 2013). The concentrations of recycled kerogen have not been well studied, but in one instance, recycled kerogen (and graphite) has been identified in sediments depositing from rapidly uplifting terrains of Southern Taiwan (Sparkes and others, 2020). The concentrations of recycled kerogen were not determined, but they might be relatively high due to the incomplete oxidative weathering organic matter in soils experiencing rapid uplift (Bolton and others, 2006).

The half saturation constant, *km* is also important in determining the kinetics of the oxygen-dependent oxidation of organic carbon in sedimentary rocks. There is little data on petrographic carbon oxidation kinetics, but in one experimental study, the oxygen-dependency of coal carbon oxidation was explored (Chang and Berner, 1999). When results from this study were analyzed with a Michaelis-Menten model, a *km* value of 0.2 PAL was determined (Bolton and others, 2006). Furthermore, when the oxidation kinetics from Chang and Berner (1999) were applied to a soil weathering model (Bolton and others, 2006), petrographic carbon was fully oxidized with atmospheric oxygen concentrations of 0.25 PAL and the mean continental erosion rate of 5 cm ky^{-1} (Holland, 1978).

The complete oxidation of petrographic carbon is not fully consistent with its recycling during weathering as discussed above. Therefore, the present model is calibrated to recycle 0.04 wt% of high maturity carbon (the equivalent of graphite) in modern marine sediments at 0.25 PAL. This calibration determines the value of *Rmaxh*, representing the maximum oxidation rate of high-maturity terrestrial carbon. The value of *Rmaxl*, representing the maximum oxidation rate of low-maturity terrestrial carbon, is determined with the same values of *km* and PAL, but assuming that this low-maturity carbon (the equivalent of kerogen) is also recycled into marine sediments with a concentration of 0.04 wt% (giving a total of 0.08 wt% recycled petrographic carbon). To accomplish this calibration, the model was run through all of Earth history and by fixing Phanerozoic Eon oxygen levels at 0.25 PAL (higher levels of oxygen produce no further organic carbon oxidation), while Neoproterozoic levels were fixed at 0.1 PAL. With the kinetics of the rock cycle as modeled here, the history of oxygen before 1000 Ma has little bearing on the organic carbon dynamics of modern sediments. With these input parameters, values of *Rmaxh* of 1.2 and *Rmaxl* of 1.7 were determined. All subsequent model runs will use these values. While the amount of recycled petrographic carbon in modern sediments is not obviously coupled to the modeling the early-Earth carbon cycle, this value is needed to calibrate the oxygen-dependent organic matter oxidation kinetics during weathering as explored above.

Isotope Mass Balance

All organic carbon and inorganic carbon in this model adopt an isotopic composition at the time they are newly deposited onto marine sediments, and they maintain

these isotopic compositions through subsequent rock cycling and weathering. The isotopic composition of the input CO_2 from the mantle, *delmantle*, is assumed to have been constant with a $\delta^{13}C$ of -5‰, consistent with assumptions of the mantle value (Deines, 1980; Des Marais and others, 1992). While the subduction of carbon is implicit in the present model, it is assumed that subducted carbon, on average, maintains the mantle $\delta^{13}C$ of -5‰. This may not be completely correct as CO_2 emerging from modern volcanic arcs have variable, but average, $\delta^{13}C$ values slightly more ^{13}C-enriched than this at -3.8‰ to -4.6‰ (Mason and others, 2017). How the $\delta^{13}C$ input of CO_2 from convergent boundaries might have changed over time is unknown. However, changing the mantle input value, especially by small amounts, would have little influence on the conclusions offered here. Therefore, it is assumed that through Earth history, the isotopic composition of all carbon in the Earth surface reservoir has had a constant $\delta^{13}C$ of -5‰, although the isotopic compositions of carbon in individual reservoirs vary as a function of rock and carbon cycling as explored below.

As noted above, the model begins with the input of CO_2 from the mantle. This carbon forms organic matter and inorganic carbon based on the value of *forg* as described above, while the isotopic difference between inorganic carbon and inorganic carbon depends on a fractionation factor, *frac:*

$$frac = (\delta^{13}Cic - \delta^{13}Coc) \qquad (19)$$

Assuming that $\delta^{13}Cic \equiv \delta^{13}Csw$ (the $\delta^{13}C$ of seawater), Equation 19 is combined with Equation 2 and rearranged so that:

$$\delta^{13}Cic \; \equiv \delta^{13}Csw \; = frac * forg + \delta^{13}Cin \qquad (20)$$

In standard modeling, a value for *frac* of 25 ‰ will be used. This value is compatible with the Archean and Paleoproterozoic carbon isotope record (Krissansen-Totton and others, 2015), although other values will be explored in a sensitivity analysis.

In the initial step of the model, $\delta^{13}Cin$ is taken as the mantle value, *delmantle*. From here, as noted above, all carbon follows through the rock cycle with isotopic compositions inherited when the carbon initially deposited into marine sediments. Thus, each carbon pool carries an isotopic composition distinct from the others and a product of its specific history of cycling and recycling. In these subsequent time steps, $\delta^{13}Cin$, becomes *delFItm* (see table 2), the isotopic composition of inorganic carbon input to the Earth surface, which is the sum of the isotopic signal of all weathering, degassing and metamorphism processes specific to each individual time step. The value of *delFItm* can vary greatly from the mantle value. All mass balance equations can be found in the interactive model in the supplemental Excel sheet (http://earth.geology.yale.edu/%7eajs/SupplementaryData/2021/Canfield). As part of the model development, and before implementation, it was verified that the model maintained mass balance with respect to rock and sediment mass, carbon mass, and carbon isotopes.

<div align="center">MODEL RESULTS AND DISCUSSION</div>

<div align="center">*Carbon Isotope Record*</div>

Model results will be compared to, and calibrated with, the carbonate carbon isotope record (Krissansen-Totton and others, 2015). It is well-known that the carbon isotope record can be subject to a variety of processes that can alter $\delta^{13}C$ values from those originally deposited with the sediment. These processes include the diagenetic

recrystallization of carbonates through fluid interactions with waters containing a different isotopic value (for example, Lohmann, 1988; Swart, 2015; Hoffman and Lamothe, 2019). Furthermore, carbonates can be incorporated into sediments by different processes including primary precipitation from seawater (either biologically or abiologically mediated) and through early sediment diagenesis. During early diagenesis, the isotopic composition of sediment pore waters plays a significant role in establishing the isotopic composition of the precipitated carbonate (for example, Fischer and others, 2009; Blanchet and others, 2012; Schrag and others, 2013; Canfield and others, 2018; Canfield and others, 2020). Furthermore, benthic photosynthesis and associated respiration can impact the isotopic composition of carbonates precipitated directly on the seafloor (Geyman and Maloof, 2019), while both lateral and vertical gradients in the isotopic composition of marine inorganic carbon can generate variability in the isotopic composition of marine carbonates precipitated contemporaneously from seawater (Hilting and others, 2008). The carbon isotope record can also vary substantially over time intervals ranging from hundreds of thousands to millions of years (for example, Halverson and others, 2005; Saltzman and Thomas, 2012; Canfield and others, 2020). Such variability could generate significant time correlation issues early in Earth history where biostratigraphy is impossible and where chronology is relatively imprecise.

The isotope record of marine carbonates used in subsequent modeling (fig. 3) shows a few prominent features including a trend of relatively stable $\delta^{13}C$ values of around 0‰ from 3500 to about 2500 Ma. From here, $\delta^{13}C$ values become more variable through the Huronian glaciations (2450–2220 Ma) after which they become highly elevated during the subsequent Lomagundi isotope event. Altogether, there are relatively few $\delta^{13}C$ data considering the vast stretch of geologic time represented (*ca.* 1/3 of Earth history). Still, as a first-order assumption, we assume these values reflect, at least approximately, the isotopic composition of contemporaneous seawater. The modeling considers broad trends in carbon cycle evolution, and while the issues related to the integrity of the carbon isotope record as noted above are significant, the assumption of seawater equivalence does not mean that every point need represent a seawater value, it only requires that average values through protracted periods of time do. This assumption seems reasonable. We also note that for the prominent Lomagundi isotope event, the large positive $\delta^{13}C$ excursion is known from multiple locations and seems to reflect a real evolution in seawater $\delta^{13}C$ values (Melezhik and others, 2005; Bekker and others, 2006; Maheshwari and others, 2010). The range of values represented in this event, however, is large, and in some instances, isotope values may reflect some facies control (for example, Melezhik and others, 2005). Therefore, the extreme values may overemphasize the true magnitude of the event (Melezhik and others, 2005). For this reason, our target during the Lomagundi isotope event is approximately 5 permil, an approximate average of values through this event.

Pre-GOE Carbon Burial

The model is grounded in the basic assumption that levels of atmospheric oxygen before the GOE were low, and for modeling purposes, a value of 0.00001 PAL was used. As noted above, "whiffs" of somewhat elevated oxygen levels may have punctuated middle and late Archean times (for example, Anbar and others, 2007; Wille and others, 2007; Crowe and others, 2013). The oxygen levels required, however, to produce the geochemical signals representing these oxygen "whiffs" could have been in the range of 0.0001 to 0.001 PAL (Johnson and others, 2019). Even these elevated oxygen levels would not have influenced model results given the relatively high *km* value
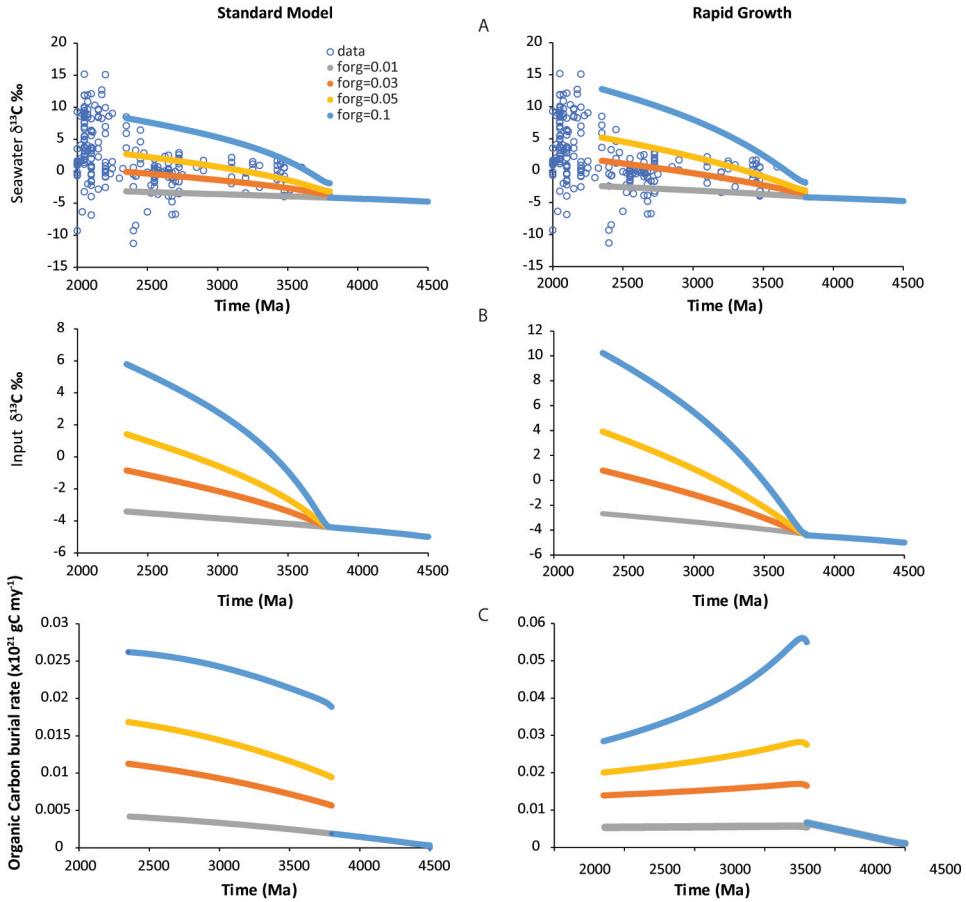
Fig. 3. (A) comparing model results for the $\delta^{13}C$ of seawater from the Standard Model with the Rapid Growth model with different values of *forg* compared to the carbon isotope record. Atmospheric oxygen concentrations were held to 0.00001 PAL. (B) Model results for the $\delta^{13}C$ of the inorganic carbon input to the oceans from the Standard Model compared to the Rapid Growth model with different values of *forg*. These values reflect, mainly, the evolution of the terrestrial inorganic carbon pool. Atmospheric oxygen concentrations were held to a PAL of 0.00001. (C) Organic carbon burial rates in the oceans the oceans from the Standard Model compared to the Rapid Growth model with different values of *forg*. Atmospheric oxygen concentrations were held to a PAL of 0.00001. Breaks in the curves result from changes in model input parameters.

for the oxidation of rock-hosted carbon (0.2 PAL). Indeed, much higher values of oxygen (up to 0.01 PAL) could have been used with an almost identical result.

We do not know when life first evolved on Earth or when biologically produced isotopically depleted carbon first deposited into marine sediments. But, as noted above, this likely occurred before deposition of ^{13}C-depleted carbon in *ca.* 3800 Ma sedimentary rocks from Isua, Greenland (Rosing, 1999). Given our ignorance as to when life first evolved, a low *forg* of 0.01 was used for the time before 3800 Ma, consistent with a biosphere that fixed very little carbon compared to the carbon flowing through the Earth surface system. This value of *forg* is low enough to have only a small influence on the carbon cycle. From here, values of *forg* were adjusted in the pre-GOE time window from 3800 to 2350 Ma, and constrained by comparison with the carbon isotope record (Krissansen-Totton and others, 2015).

Results from both the Standard and Rapid Growth model are similar and show that an *forg* = 0.1, a value considerably lower than the 0.17 to 0.25 obtained with a strict interpretation of the carbon isotope record as discussed above, does a poor job of reproducing the carbon isotope record (fig. 3A). The isotope record is not reproduced because in the absence of the oxidative weathering of organic carbon on land, the isotopic composition of inorganic entering the oceans from land, *delFItm*, becomes ^{13}C-enriched compared to the mantle value (fig. 3B), thus enriching the δ^{13}C of seawater in the absence of significant organic matter formation. Overall, in the absence of oxidative weathering of organic carbon on land, the Archean and early Paleoproterozoic isotope record must be interpreted with caution.

We see that for both models, the best fit to the isotope data occurs with an *forg* of around 0.03, especially in the late Archean isotope record (fig. 3A). An *forg* of 0.01 does not generate a sufficiently ^{13}C-enriched isotope signal, while an *forg* of 0.05 slightly overestimates the δ^{13}C values of the isotope record, particularly in the late Archean Eon, with a somewhat worse fit with the Rapid Growth model. Mixed models were also explored where the growth of the carbon reservoir from the Standard Model was combined with the growth of the sedimentary rock reservoir of the Rapid Growth model, and vice versa. It was found (not shown) that the carbon growth model drove the results and that growth of the sedimentary rock reservoir had little influence on the model output parameters depicted in figure 3. These mixed models were explored no further.

Modeled rates of organic carbon burial into marine sediments are shown in figure 3C. These burial rates are those associated with contemporaneous primary production in the oceans and do not include the recycling of organic carbon from land. From these results, and with an *forg* of 0.03, rates of organic carbon burial depend very much on the crustal growth model especially during the Archean Eon. In the Standard Model, a change in *forg* from 0.01 to 0.03 results in an immediate increase in organic carbon burial rates from about 0.005×10^{21} g my^{-1} in the early Archean Eon, to a value of about 0.01×10^{21} g my^{-1} just before the GOE. These rates of carbon burial amount to about 4 percent of the modern burial rate of about 0.12×10^{21} g my^{-1} (Baturin, 2007) at 3800 Ma and about 8 percent of this rate at 2350 Ma. With the Rapid Growth model, early Archean rates of organic carbon burial are much higher at about 0.016×10^{21} g my^{-1} reflecting the rapid growth of the carbon reservoir. From here, the rates decrease to about 0.012×10^{21} g my^{-1} reflecting the redistribution of carbon into the various compartments of the rock cycle. Even at their highest, these rates of carbon burial are about 13 percent as nigh as modern rates of carbon burial. Overall, these models predict rates of pre-GOE carbon burial that were some 4 percent to 13 percent as rapid as modern rates.

We also explored the Hayes and Waldbauer (2006) (H and W) carbon accumulation model (fig. 4). During pre-GOE times, this model yields similar results to the Standard Model, but an *forg* of 0.05 better fits the isotope data. However, this higher *forg* generates similar carbon burial rates to the Standard Model (with an *forg* of 0.03) in pre-GOE times as the H and W model introduces less carbon into the early Earth surface environment (fig. 1). The H and W GOE model results will be discussed below.

In a sensitivity analysis, *MetaM*, the fraction of organic matter liberated to CO_2 during metamorphism, was also varied between values of 0.2 to 0.8 (fig. 5). All model calculations were performed with an *forg* of 0.03 for the time window between 3800 and 2350 Ma, an *frac* of 0.01 from 4500 Ma to 3800 Ma and an oxygen level of 0.00001 PAL. It is clear pre-GOE, changing *MetaM* had little influence on both the isotope fit (fig. 5A), as well as organic carbon burial rates (fig. 5B). There was a change, however, in the input δ^{13}C to the oceans, where higher degrees of metamorphic CO_2 liberation
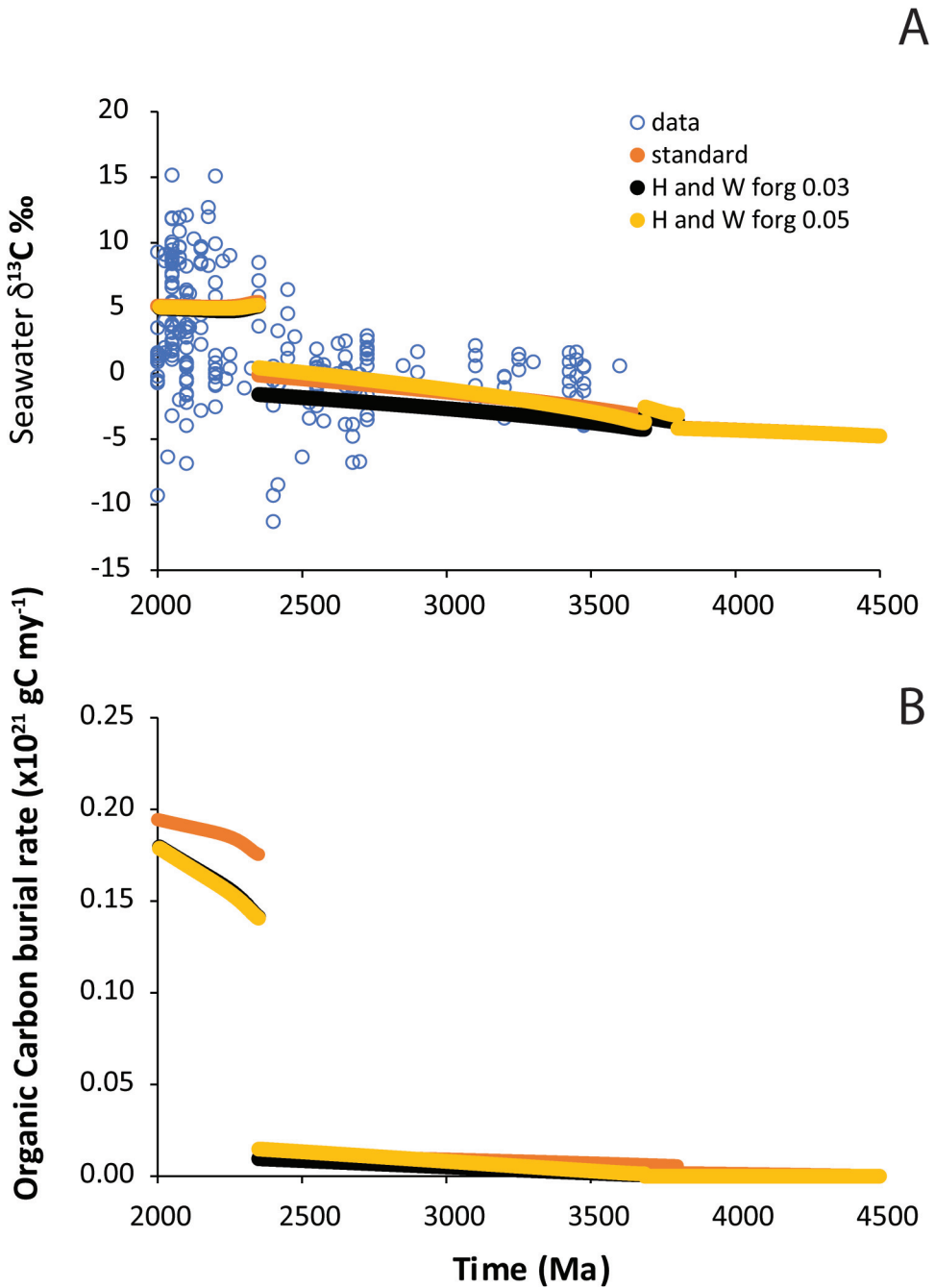
Fig. 4. Results from the Hayes and Waldbauer (H and W) model of continental growth compared to the Standard Model. For pre-GOE times, atmospheric oxygen was set to 0.00001 PAL, and *forg* was set to 0.03 in the standard model, while various values of *forg* were explored for the H and W model. For the GOE and Lomagundi isotope event, atmospheric oxygen was set to 0.25 PAL and *forg* was set to 0.4 for all models. (A) Evolution of seawater δ^{13}C, and (B) evolution of the organic carbon burial rate into marine sediments. Breaks in the curves result from changes in model input parameters.
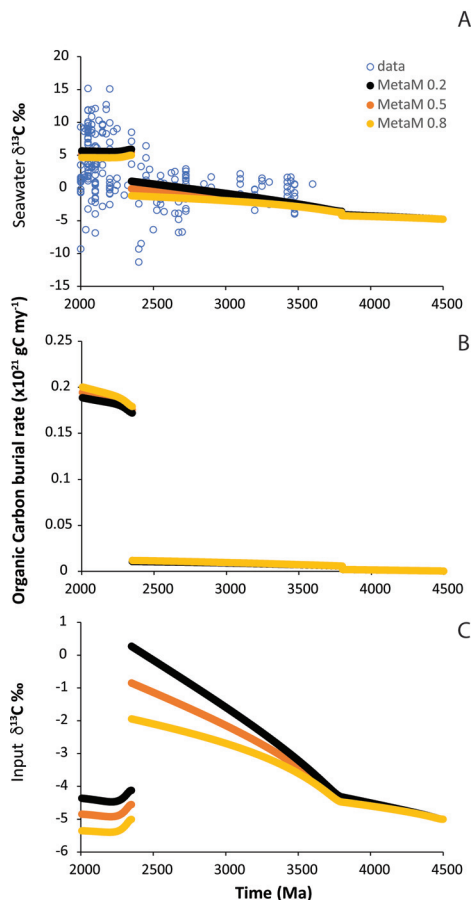
Fig. 5. Sensitivity analysis comparing different values for the metamorphic release of carbon to the Earth surface during metamorphism through the variable *MetaM*. For pre-GOE times, atmospheric oxygen was set to 0.00001 PAL, and *forg* was set to 0.03. For the GOE and the Lomagundi isotope event, atmospheric oxygen was set to 0.25 PAL and *forg* was set to 0.4 for all models. A value of *MetaM* of 0.5 is the same as used in the Standard Model. (A) Evolution of seawater δ^{13}C, (B) evolution of the organic carbon burial rate into marine sediments, (C) isotopic composition of inorganic carbon entering the Earth surface as a product of weathering, degassing and metamorphic carbon release. Breaks in the curves result from changes in model input parameters.

generated more ^{13}C-depleted CO_2 (fig. 5C). In another sensitivity analysis, the fractionation factor, *frac*, between the inorganic carbon precipitated from the oceans and the organic carbon forming in sediments was varied between 20 permil and 30 permil (fig. 6). Changing of *frac* through this range had little influence on fitting the pre-GOE isotope record (fig. 6A), with some influence on the δ^{13}C input carbon to the oceans (fig. 6B). Higher fractionations produced more ^{13}C-enriched input to the oceans as higher fractionations produced more ^{13}C enriched carbonates precipitated onto marine sediments. Changing the fractionation factor had no influence on the burial rates of organic carbon, so these results are not shown.

Overall, model results generate low rates of pre-GOE organic carbon burial and might suggest low pre-GOE rates of primary production and thus a sluggish biosphere. Overall, however, the extent to which rates of carbon burial can be compared to rates of primary production depends on the efficiency with which primary
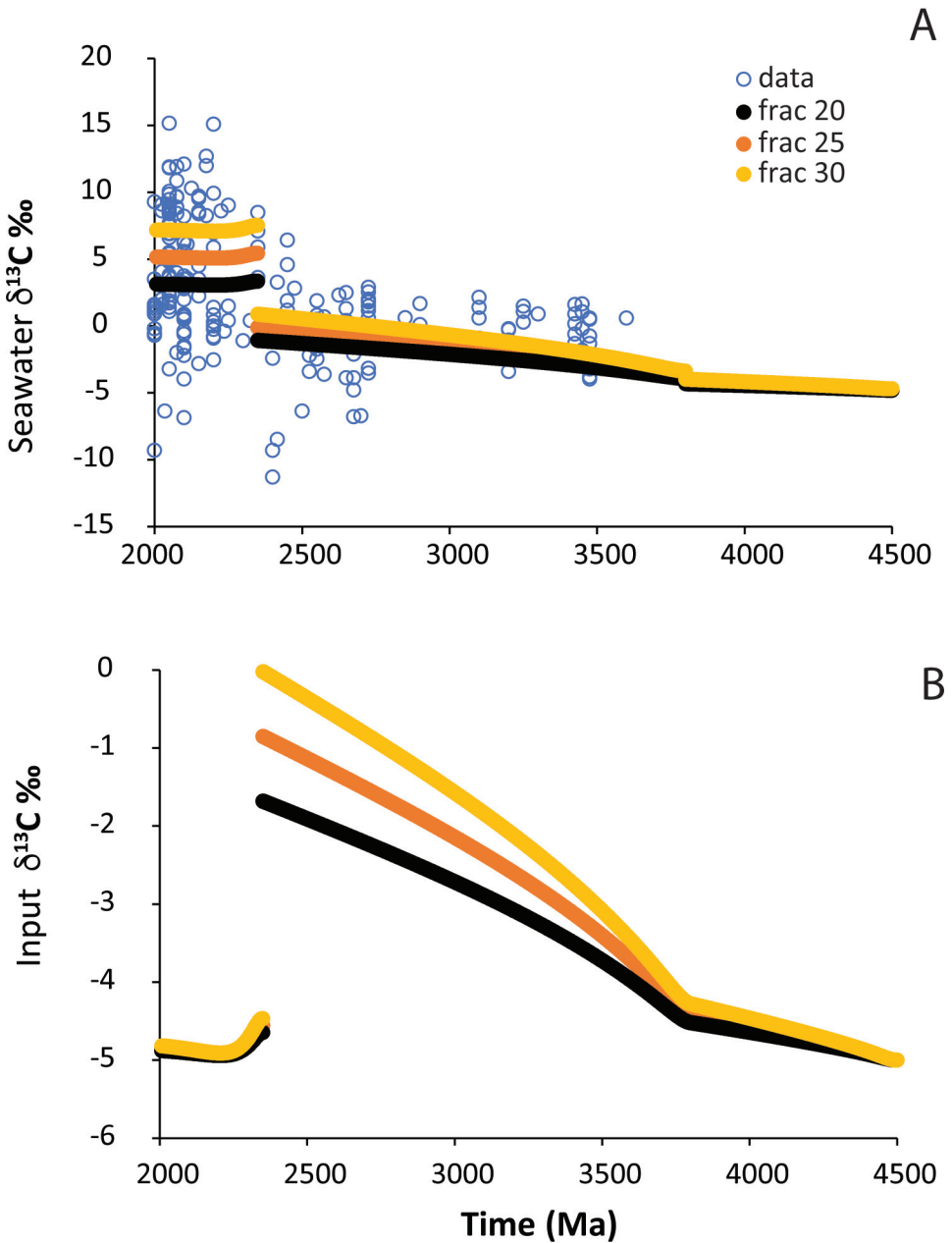
Fig. 6. Sensitivity analysis comparing different values for the fractionation, *frac*, between organic matter and inorganic carbon during primary production in the oceans. For pre-GOE times, atmospheric oxygen was set to 0.00001 PAL, and *forg* was set to 0.03. For the GOE and the Lomagundi isotope event, atmospheric oxygen was set to 0.25 PAL and *forg* was set to 0.4 for all models. A value for *frac* of 25‰ is the same as used in the Standard Model. (A) Evolution of seawater $\delta^{13}C$, (B) isotopic composition of inorganic carbon entering the Earth surface as a product of weathering, degassing and metamorphic carbon release. Breaks in the curves result from changes in model input parameters.

produced carbon is transferred for burial into sediments. This, in turn, can depend on many factors, including, most importantly, the settling rates of organic matter through the water column and the efficiency of organic matter decomposition during settling in the water column and within sediments during diagenesis (for example, Zhang and others, 2016; Fakhraee and others, 2020). If settling is slow, as might be expected with an ecosystem constructed of small prokaryotic organisms (Logan and others, 1995), then more extensive water-column organic matter mineralization might lead to more nutrient availability, boosting primary production and thus elevating rates of primary production relative to rates of carbon burial. If, on the other hand, rates of organic matter mineralization are reduced under anoxic water column and sediment conditions as might be expected on a low-oxygen Earth, then rates of primary production might be reduced relative to rate of organic carbon burial (Laakso and Schrag, 2019; Fakhraee and others, 2020). The balance of these two drivers is not fully resolved, and for the purpose of the present discussion, it will be assumed that rates of primary production, and thus the activity of the biosphere, scales at least approximately with carbon burial rates.

Therefore, the results presented here are viewed as compatible with a subdued pre-GOE biosphere when compared to the biosphere today. There could be many explanations for a subdued pre-GOE biosphere. These explanations include phosphorus limitation, where in one estimate, limited phosphorus availability in the late Archean Eon could have supported rates of net primary production of only about 7 percent of present-day rates (Hao and others, 2020). This estimate is remarkably close to the estimate here using the Standard Model of late-Archean organic carbon burial rates compared to modern rates as discussed above. Another explanation could lie in the state of biological evolution and the nature of primary-producing organisms in the pre-GOE world. For example, if cyanobacteria had not yet evolved before the GOE, as discussed above, rates of biological productivity would have been necessarily lower due to a lack of suitable electron donors to fuel primary production. The activity level of the biosphere before the evolution of cyanobacteria is highly uncertain, but as noted above, a biosphere based on the recycling of iron, as was likely important during the Archean and early Proterozoic Eons (for example, James, 1983; Beukes and Klein, 1992; Konhauser and others, 2002; Konhauser and others, 2017) could have provided rates of net primary production up to 10 percent of present-day rates. Thus, cyanobacteria may not have been necessary to generate the pre-GOE burial rates or organic carbon as calculated here.

THE GOE AND LOMAGUNDI ISOTOPE EVENT

The Great Oxidation Event, or GOE, marks a profound change in the oxidation level of the Earth-surface environment, where atmospheric oxygen levels rose to concentrations sufficient for significant oxidative weathering of redox-sensitive minerals on land (for example, Cloud, 1972; Holland, 1994; Holland, 1999; Melezhik and others, 1999b). The GOE is commonly marked by the loss of the mass-independent sulfur (MIF) isotope signal in the sedimentary sulfur record, indicating the full oxidation of atmospheric SO_2 gas to sulfate (for example, Farquhar and others, 2000; Pavlov and Kasting, 2002; Bekker and others, 2004; Warke and others, 2020). The earliest indication for the loss of the MIF signal loss is between 2501 and 2434 Ma, immediately preceding the first of the Paleoproterozoic Huronian glaciations (Warke and others, 2020). There are indications of a positive $\delta^{13}C$ excursion to about 6 ‰ to 8 ‰ in the Duitschland Formation of the *ca.* 2400 Transvaal Supergroup of South Africa (Buick and others, 1998), and there is a large and sustained positive $\delta^{13}C$ excursion, known as the Lomagundi isotope event, lasting from about 2300 to 2060 Ma, as introduced above. The Lomagundi isotope event follows the end of the Huronian

glaciations (for example, Karhu and Holland, 1996; Melezhik and others, 1999b; Maheshwari and others, 2010; Lajoinie and others, 2019), with the δ^{13}C of many carbonate values exceeding 10 ‰. Near the end of this event is the deposition, in some locations, of extremely organic rich sediments known as shungite (Melezhik and others, 1999a; Melezhik and others, 2004).

High concentrations of atmospheric oxygen have been inferred for the Lomagundi isotope event (Bekker and Holland, 2012), and in one model exercise, oxygen levels of between about 0.67 and 2 times PAL are indicated (Bachan and Kump, 2015). Elevated oxygen levels through this time period, and especially through the Lomagundi event, are supported by evidence for high enrichments of uranium in shales (Partin and others, 2013), elevated concentrations of iodine in carbonates (Hardisty and others, 2014), elevated δ^{98}Mo values in shales (Canfield and others, 2013) and abundant sulfate evaporites (Schröder and others, 2008; Blättler and others, 2018). In the modeling that follows, a GOE and post-GOE oxygen level of 0.25 PAL will be used, as higher oxygen levels produce no further organic carbon oxidation during weathering. The consequences of lower oxygen levels, however, will also be explored.

Thus, the modeling of the GOE and Lomagundi events entails following the consequences of increased oxygen concentrations on the carbon cycle. By doing so, the model aims to reproduce the carbon isotope record and to constrain burial rates of organic carbon, allowing comparisons between the activity level of the GOE and post-GOE biospheres with the pre-GOE biosphere as modelled above. If we take 5 permil as a reasonable fit to the late GOE and Lomagundi isotope record (as discussed above), then with 0.25 PAL oxygen, an *forg* of 0.4 is required to match the isotope record (fig. 7A). This is true for the Standard Model, the Rapid Growth model (fig. 7A) and the H and W model (fig. 4A). An elevated *forg* for the GOE, and especially the Lomagundi isotope event, is consistent with previous modelling of the isotope record (Karhu and Holland, 1996; Bjerrum and Canfield, 2004; Krissansen-Totton and others, 2015; Miyazaki and others, 2018). The present modelling, however, shows that an increase in *forg* through and after the GOE, combined with an increase in the flux of inorganic carbon to the oceans as generated from high oxygen levels, results in increases in organic carbon burial rate by over a factor of 10 (figs. 4 and 7) compared to pre-GOE values.

Reducing PAL to 0.1 hinders the oxidation of organic carbon on land (see below), raising the δ^{13}C of the inorganic carbon input to the oceans (fig. 7B). Preserving an *forg* of 0.4 produces an increase in the δ^{13}C of seawater (figs. 5A and 6A) compared to when PAL is 0.25, and with a PAL of 0.1, modeled δ^{13}C values are in the upper range of those observed during the Lomagundi isotope event. With an *forg* of 0.4, organic carbon burial rates are marginally reduced with 0.1 PAL oxygen compared to 0.25 PAL (fig. 7C). Thus, even with oxygen levels of 0.1 PAL, the model here suggests that organic carbon burial rates were some 80 percent of those reproduced at 0.25 PAL in both the Standard and Rapid Growth models. All models suggest carbon burial rates on the order of 0.16 to 0.23 × 10^{21} gC my^{-1} (figs. 4, 5, and 7).

The W and H carbon accumulation model yields nearly identical carbon isotope fits to the δ^{13}C record with the same input parameters of PAL (0.25) and *forg* (0.4), with slightly reduced rates of carbon burial (fig. 4), reflecting a somewhat smaller carbon inventory at this time (fig. 1). Changing *MetaM* has only a small effect on the carbon isotope fit to the δ^{13}C record and also has little impact on carbon burial rates, although the input δ^{13}C to the oceans is somewhat affected (fig. 5). Changing *frac* influences the fit to the δ^{13}C record. With the same input parameters of PAL (0.25) and *forg* (0.4), a *frac* value of 20 permil produces lower δ^{13}C values than the standard fit with a *frac* of 25 permil, and a *frac* of 30 permil produces higher δ^{13}C values than in the standard model (fig. 6). To reproduce a seawater δ^{13}C of -5‰, the *frac* 20 permil
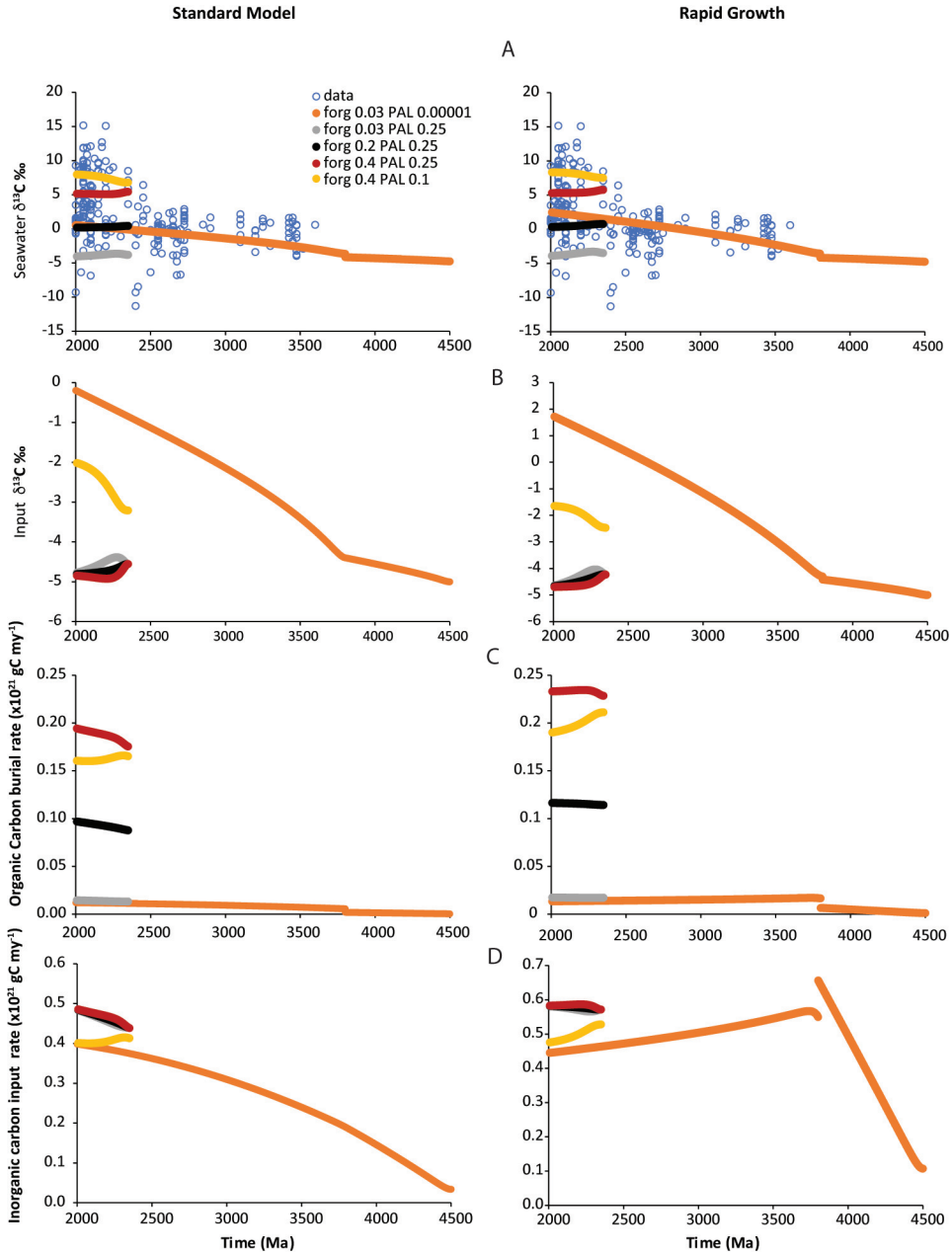
Figure 7. (A) Model results for the $\delta^{13}C$ of seawater from the Standard and Rapid Growth models with different values of *forg* and PAL, with focus on GOE and post-GOE times compared to the carbon isotope record. Also shown for comparison is the Standard and Rapid Growth model results with *forg* = 0.03 and PAL = 0.00001. (B) Model results for the $\delta^{13}C$ of the inorganic carbon input to the oceans from the Standard and Rapid Growth models with different values of *forg* and PAL, with focus on GOE and post-GOE times. Also shown is the Standard and Rapid Growth model results with an *forg* = 0.03 and PAL = 0.00001. (C) Organic carbon burial rates in the oceans from the Standard and Rapid Growth models with different values of *forg* and PAL, with focus on GOE and post-GOE times. Also shown is the Standard and Rapid Growth Model results with an *forg* = 0.03 and PAL = 0.00001. (D) Evolution of the input rates of inorganic carbon to the oceans from the Standard and Rapid Growth models with different values of *forg* and PAL, with a focus on GOE and post-GOE times. Also shown is the Standard and Rapid Growth Model results with an *forg* = 0.03 and PAL = 0.00001. Breaks in the curves result from changes in model input parameters.

model would need an *forg* of 0.48 generating an organic carbon burial rate of 0.23×10^{21} gC my^{-1} at 2000 Ma (not shown). The *frac* 30 permil model would need an *forg* of 0.33 producing an organic carbon burial rate of 0.16×10^{21} gC my^{-1} at 2000 Ma (not shown). These organic matter burial rates are all within the estimates for Lomagundi event as outlined above.

Carbon Cycle Evolution

The discussion above provides a general picture as to how changing oxygen levels and *forg* have influenced the evolution of the carbon cycle. However, it is also instructive to analyze all components of the carbon cycle to appreciate how they respond individually to changes in PAL and *forg*. To do this, we follow the carbon cycle through its whole course of evolution from pre-GOE times through the Lomagundi isotope event. We explore the case where PAL increases from 0.00001 to 0.25 through the GOE and *forg* increases from 0.03 to 0.4 through the same transition. The results for both the Standard Model and the Rapid Growth model are quantitatively and qualitatively similar (figs. 8 and 9). In pre-GOE times, most of the organic matter depositing into marine sediments (figs. 8A and 9A) was recycled from land particularly as low maturity carbon (*Cml*), but with increasing amounts of high maturity carbon (*Cmh*) towards the GOE. The increase in PAL and *forg* in association with the GOE resulted, first, in efficient oxidation of organic matter in rocks during weathering and hence a large reduction in the delivery of recycled petrographic to marine sediments. This reduction in the delivery of recycled carbon dramatically decreased its concentration in the marine sediment pool (figs. 8A and 9A). In association with the increase in *forg*, newly produced marine organic matter came to dominate the organic carbon pool in marine sediments. An increase in the production of organic carbon in the oceans reduced the deposition of inorganic carbon as evidenced by its decreased concentration in marine sediments (figs. 8G and 9G).

As the large flux of newly formed marine organic matter associated with the GOE was transported onto land, the concentrations of low-maturity carbon in the terrestrial pool of young rocks (*Ctyl*) increased. There was also a decrease in the concentration of high maturity carbon (*Ctyh*) in the young terrestrial pool (figs. 8C and 9C) as would be expected with an increase in oxygen concentrations and the reduced recycling of high maturity carbon into marine sediments. As the young terrestrial pool matured to the old terrestrial pool, there was an increase in the concentration of low-maturity carbon in the old terrestrial pool of low thermal grade (*Ctoll*) as well as the expected decrease in the concentration of high maturity carbon in the old terrestrial pool of low-thermal grade (*Ctohl*) (figs. 8E and 9E). As organic carbon in low maturity old terrestrial rocks was metamorphosed, a portion of it (minus the portion that was lost as CO_2) was converted to high maturity carbon (*Ctoh*), and this pool increased in association with the GOE (figs. 8E and 9E). Some high-maturity recycled carbon was also transferred without metamorphic effect from the low-maturity rocks. The isotopic consequences of these transformations are nearly identical between the Standard Model and the Rapid Growth models (compare figs. 8B, 8D, 8F, and 8H with figs. 9B, 9D, 9F, and 9H).

An Active GOE and Lomagundi Biosphere

If we accept that the GOE, and especially the Lomagundi isotope event, was associated with oxygen levels of greater than 0.1 PAL, as would be consistent with modeling (Bachan and Kump, 2015), then regardless of the Earth-surface carbon inventory model we use, the GOE was accompanied by a dramatic change in the burial rates of organic matter. Indeed, modeling suggests that organic carbon burial rates were on the order of 0.16 to 0.23×10^{21} gC my^{-1} (figs. 4 and 7). These rates are some 13 to 19 times greater than during pre-GOE times (figs. 3 and 4) and 1.3 to 1.9 times greater

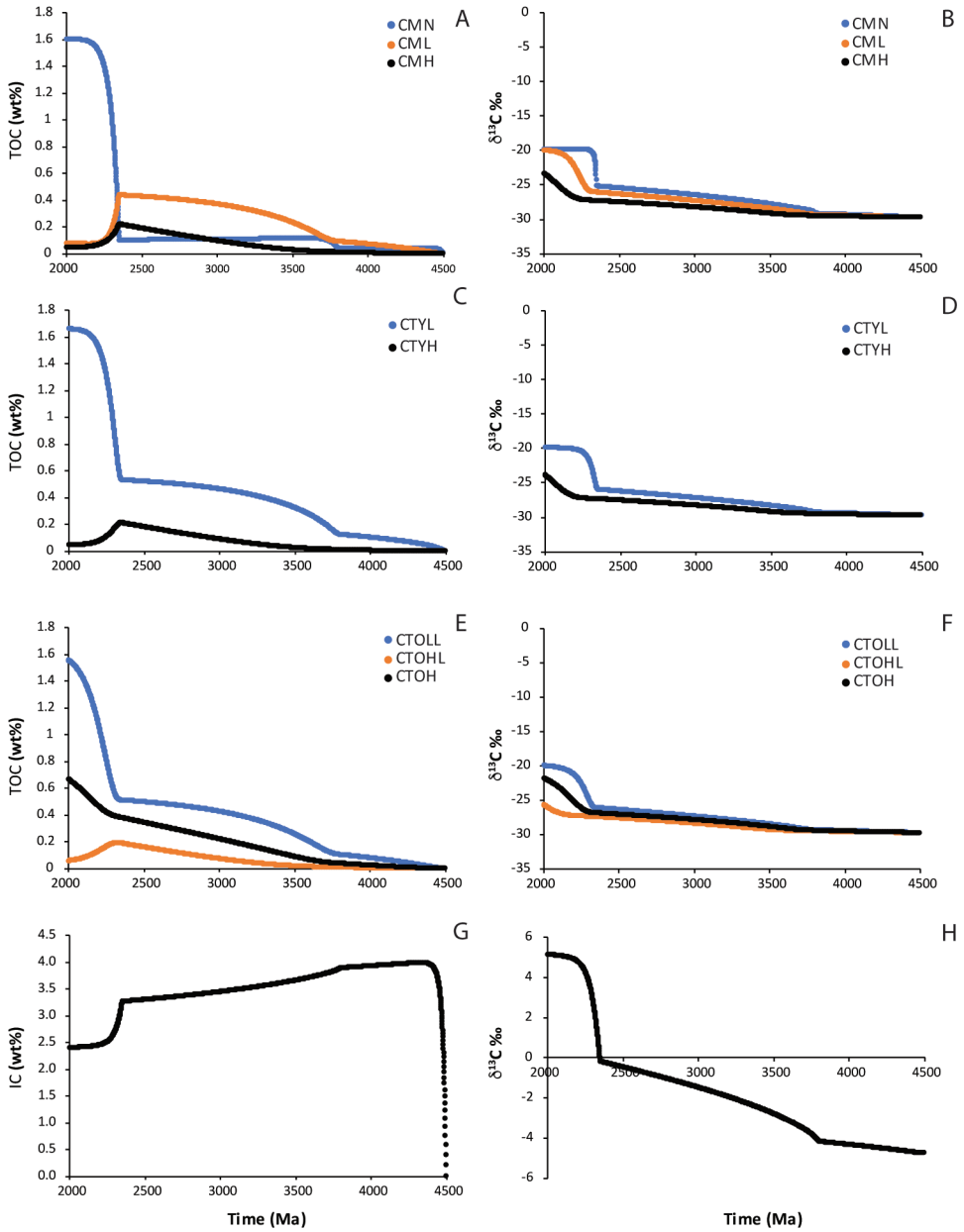Fig. 8. Model results for the time evolution of different components of the rock cycle for the "Standard Model" with a transition from *forg* = 0.03 and PAL = 0.00001 at 2400 Ma to *forg* = 0.4 and PAL= 0.25. (A) Evolution of the concentrations of various organic matter pools in marine sediments, (B) evolution of the isotopic compositions of various organic matter pools in marine sediments, (C) evolution of the concentrations of various organic matter pools in the young terrestrial reservoir, (D) evolution of the isotopic compositions of various organic matter pools in the young terrestrial reservoir, (E) evolution of the concentrations of various organic matter pools in the old terrestrial reservoir, (F) evolution of the isotopic compositions of various organic matter pools in the old terrestrial reservoir, (G) evolution of the concentrations of inorganic carbon in marine sediments, (H) evolution of the isotopic composition of inorganic carbon in marine sediments. See text for details.
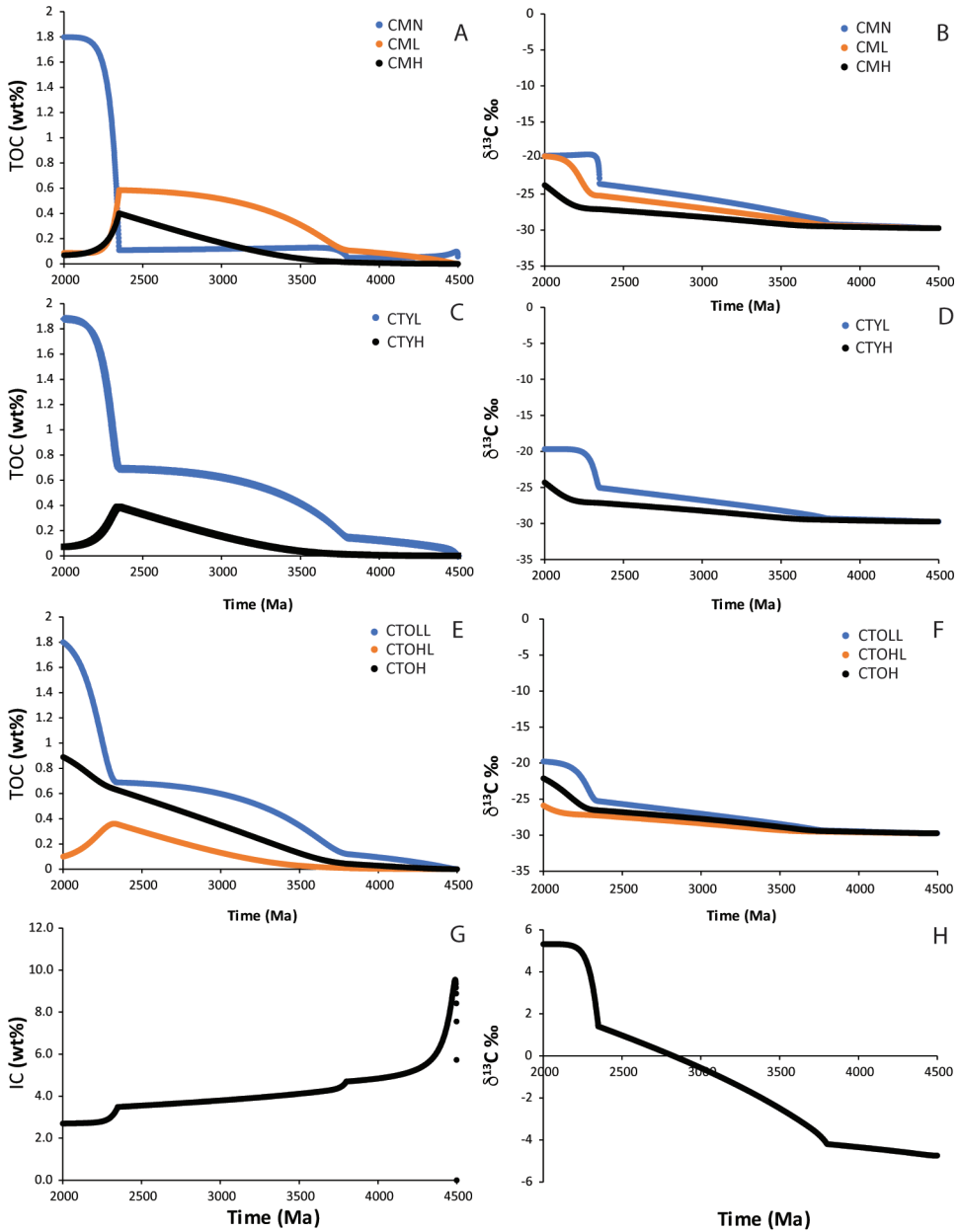
Fig. 9. Model results for the time evolution of different components of the rock cycle for the Rapid Growth model with a transition from *forg* = 0.03 and PAL = 0.00001 at 2400 Ma to *forg* = 0.4 and PAL = 0.25. (A) Evolution of the concentrations of various organic matter pools in marine sediments, (B) evolution of the isotopic compositions of various organic matter pools in marine sediments, (C) evolution of the concentrations of various organic matter pools in the young terrestrial reservoir, (D) evolution of the isotopic compositions of various organic matter pools in the young terrestrial reservoir, (E) evolution of the concentrations of various organic matter pools in the old terrestrial reservoir, (F) evolution of the isotopic compositions of various organic matter pools in the old terrestrial reservoir, (G) evolution of the concentrations of inorganic carbon in marine sediments, (H) evolution of the isotopic composition of inorganic carbon in marine sediments. See text for details.

than the modern organic matter burial rate of 0.12×10^{21} gC my^{-1} (Baturin, 2007). This dramatic increase in organic matter burial was most likely coupled to a dramatic increase in rates of primary production and the overall activity level of the biosphere. Thus, if we assume that rates of carbon burial have scaled linearly with rates of primary production through time, then the current model suggests that primary production rates during the GOE and Lomagundi events were some 1.3 to 1.9 times greater than today. In their study Crockford and others (2019) calculated that rates of gross primary production in the oceans during the GOE and the Lomagundi isotope event were approximately 10 times higher than today. Differences in the primary production estimates of Crockford and others (2019) and those offered here could be a product of uncertainties in model estimates in the different approaches or from differences in scaling between primary production and carbon burial through time. Regardless of the approach, the GOE and Lomagundi biosphere was apparently quite active, likely even more so than today, and much more active than during pre-GOE times.

An accelerated biosphere in association with the GOE could have many causes. One cause could be the evolution of cyanobacteria, where an accelerated biosphere could have resulted from the ability of cyanobacteria to use highly abundant water as an electron donor. A relationship between the evolution of cyanobacteria and the GOE has been suggested (Kirschvink and Kopp, 2008; Ward and others, 2016). Another cause for an accelerated biosphere could be an increase in the availability of nutrients, and in particular phosphorus (as noted above) in association with the rise in oxygen levels. Indeed, it has been suggested that the oxidative weathering of pyrite on land generated sufficiently acidic groundwaters to accelerate the weathering of phosphorus from rocks, thereby accelerating the activity level of the biosphere (Bekker and Holland, 2012). The current manuscript remains agnostic as to the causes of an accelerated biospheric activity during the GOE and the following Lomagundi isotope event. However, the reconstruction of the ancient carbon cycle, as developed here, suggests that the acceleration was dramatic; in a relatively short time (*ca.* one hundred million years) the biosphere seemingly increased its level activity by at least one order of magnitude.

CONCLUSIONS

Carbon cycle reconstructions based on carbon isotopes are fundamentally influenced by the oxygen dependency of organic carbon weathering. This is because in the absence of efficient oxidative weathering, a large pool of recycled organic matter sequesters isotopically depleted carbon increasing the δ^{13}C of the inorganic carbon reservoir including the dissolved inorganic carbon in the oceans. The present model, considering the oxygen-dependence of organic matter weathering and an evolving Earth-surface carbon cycle produces an *forg* of only about 0.03 for pre-GOE times, yielding carbon burial rates less than 10 percent of those in the modern oceans. Indeed, before the GOE, most the organic carbon in marine sediments was recycled as unweathered from terrestrial rocks. If the burial rates of organic carbon scaled to biological activity, then the relatively inactive pre-GOE biosphere could have been sustained by anoxygenic photosynthetic organisms driving an iron cycle. However, a relatively inactive biosphere based on oxygen production by cyanobacteria cannot be ruled out.

The GOE and subsequent Lomagundi isotope event saw a large rise in the concentrations of atmospheric oxygen to perhaps as high as 0.67 to 2 times present-day levels. From the modeling, oxygen concentrations as low as 0.1 PAL would have led to significant oxidative weathering of organic carbon on land. The GOE, and especially the following Lomagundi isotope event, saw a large increase in the δ^{13}C of inorganic

carbon precipitated from the oceans. From the current model, these isotope values are consistent with an *forg* of about 0.4 and an increase by about a factor of 10 in the burial rates of organic carbon over pre-GOE times. Such high burial rates of organic carbon suggest an active biosphere requiring oxygenic photosynthesis as a driver with abundant water as an electron donor. The substantial increase in the activity level of the biosphere through the GOE could have either been caused by the evolution or emergence of cyanobacteria as the dominant phototrophs in the environment or by an increase in the availability of nutrients to drive primary production.

ACKNOWLEDGMENTS

REFERENCES

Agirrezabala, L. M., Permanyer, A., Suárez-Ruiz, I., and Dorronsoro, C., 2014, Contact metamorphism of organic-rich mudstones and carbon release around a magmatic sill in the Basque-Cantabrian Basin, western Pyrenees: Organic Geochemistry, v. 69, p. 26–35, https://doi.org/10.1016/j.orggeochem.2014.01.014

Alcott, L. J., Mills, B. J. W., and Poulton, S. W., 2019, Stepwise Earth oxygenation is an inherent property of global biogeochemical cycling: Science (New York, N.Y.), v. 366, n. 6471, p. 1333–1337, https://doi.org/10.1126/science.aax6459

Anbar, A. D., Duan, Y., Lyons, T. W., Arnold, G. L., Kendall, B., Creaser, R. A., Kaufman, A. J., Gordon, G. W., Scott, C., Garvin, J., and Buick, R., 2007, A whiff of oxygen before the Great Oxidation Event?: Science (New York, N.Y.), v. 317, n. 5846, p. 1903–1906, https://doi.org/10.1126/science.1140325

Armstrong, R. L., 1981, Radiogenic isotopes: The case for crustal recycling on a near-steady-state no-continental-growth Earth: Philosophical Transactions of the Royal Society of London, Series A, Mathematical and Physical Sciences, v. 301, n. 1461, p. 443–472., https://doi.org/10.1098/rsta.1981.0122

Bachan, A., and Kump, L. R., 2015, The rise of oxygen and siderite oxidation during the Lomagundi Event: Proceedings of the National Academy of Sciences of the United States of America, v. 112, n. 21, p. 6562–6567, https://doi.org/10.1073/pnas.1422319112

Bao, R., Zhao, M., McNichol, A., Wu, Y., Guo, X., Haghipour, N., and Eglinton, T. I., 2019, On the origin of aged sedimentary organic matter along a river-shelf-deep ocean transect: Journal of Geophysical Research: Biogeosciences, v. 124, n. 8, p. 2582–2594, https://doi.org/10.1029/2019JG005107

Baturin, G. N., 2007, of the relationship between primary productivity of organic carbon in ocean and phosphate accumulation (Holocene-Late Jurassic: Lithology and Mineral Resources, Issue): 42, p. 318–348, https://doi.org/10.1134/S0024490207040025

Bekker, A., and Holland, H. D., 2012, Oxygen overshoot and recovery during the early Paleoproterozoic: Earth and Planetary Science Letters, v. 317–318, p. 295–304, https://doi.org/10.1016/j.epsl.2011.12.012

Bekker, A., Holland, H. D., Wang, P.-L., Rumble, D. III., Stein, H. J., Hannah, J. L., Coetzee, L. L., and Beukes, N. J., 2004, Dating the rise of atmospheric oxygen: Nature, : Nature, v. 427, p. 117–120, https://doi.org/10.1038/nature02260

Bekker, A., Karhu, J. A., and Kaufman, A. J., 2006, Carbon isotope record for the onset of the Lomagundi carbon isotope excursion in the Great Lakes area, North America: Precambrian Research, v. 148, n. 1–2, p. 145–180, https://doi.org/10.1016/j.precamres.2006.03.008

Bell, E. A., Boehnke, P., Harrison, T. M., and Mao, W. L., 2015, Potentially biogenic carbon preserved in a 4.1 billion-year-old zircon: Proceedings of the National Academy of Sciences of the United States of America, v. 112, n. 47, p. 14518–14521, https://doi.org/10.1073/pnas.1517557112

Berner, R. A., 1987, Models for carbon and sulfur cycles and atmospheric oxygen: Application to Paleozoic geologic history: American Journal of Science, p. 177–196, https://doi.org/10.2475/ajs.287.3.177

Berner, R. A., and Canfield, D. E., 1989, A new model for atmospheric oxygen over Phanerozoic time: American journal of Science, p. 333–361, https://doi.org/10.2475/ajs.289.4.333

Beukes, N. J., and Klein, C., 1992, Models for iron-formation deposition , in Schopf, J. W., and Klein, C., editors, The Proterozoic Biosphere. A multidisciplinary study: Cambridge, England, Cambridge University Press, p. 147–151.

Bjerrum, C. J., and Canfield, D. E., 2004, New insights into the burial history of organic carbon on the early Earth: Geochemistry, Geophysics, Geosystems, v. 5, n. 8, p. Q08001, https://doi.org/10.1029/2004GC000713

Blanchet, C. L., Kasten, S., Vidal, L., Poulton, S. W., Ganeshram, R., and Thouveny, N., 2012, Influence of diagenesis on the stable isotopic composition of biogenic carbonates from the Gulf of Tehuantepec oxygen minimum zone: Geochemistry, Geophysics, Geosystems: Geochemistry, Geophysics, Geosystems, https://doi.org/10.1029/2011GC003800

Blättler, C., Claire, M. W., Prave, A. R., Kirsimäe, K., Higgins, J. A., Medvedev, P. V., Romashkin, A. E., Rychanchik, D. V., Zerkle, A. L., Paiste, K., Kreitsmann, T., Millar, I. L., Hayles, J. A., Bao, H., Turchyn, A. V., Warke, M. R., and Lepland, A., 2018, Two-billion-year-old evaporites capture Earth's great oxidation: Science (New York, N.Y.), v. 360, n. 6386, p. 320–323, https://doi.org/10.1126/science.aar2687

Blattmann, T. M., Liu, Z., Zhang, Y., Haghipour, N., Montluçon, D. B., Plötze, M., and Eglinton, T. I., 2019, Mineralogical control on the fate of continentally derived organic matter in the ocean: Science (New York, N.Y.), v. 366, n. 6466, p. 742–745, https://doi.org/10.1126/science.aax5345

Bolton, E. W., Berner, R. A., and Petsch, S. T., 2006, The weathering of sedimentary organic matter as a control on atmospheric O_2: II: American Journal of Science, v. 306, n. 8, p. 575–615, https://doi.org/10.2475/08.2006.01

Buick, I. S., Uken, R., Gibson, R. L., and Wallmach, T., 1998, High-δ^{13}C Paleoproterozoic carbonates from the Transvaal Supergroup, South Africa: Geology, p. 875–878, https://doi.org/10.1130/0091-7613(1998)026<0875:HCPCFT>2.3.CO;2

Buseck, P. R., and Huang, B.-J., 1985, Conversion of carbonaceous material to graphite during metamorphism: Geochimica et Cosmochimica Acta: Geochimica et Cosmochimica Acta, p. 2003–2016, https://doi.org/10.1016/0016-7037(85)90059-6

Canfield, D. E., Rosing, M. T., and Bjerrum, C., 2006, Early anaerobic metabolisms: Philosophical transactions of the Royal Society of Londo Series B, Biological Sciences, p. 1819–1834, https://doi.org/10.1098/rstb.2006.1906

Canfield, D. E., Ngombi-Pemba, L., Hammarlund, E. U., Bengtson, S., Chaussidon, M., Gauthier-Lafaye, F., Meunier, A., Riboulleau, A., Rollion-Bard, C., Rouxel, O., Asael, D., Pierson-Wickmann, A. C., and El Albani, A., 2013, Oxygen dynamics in the aftermath of the Great Oxidation of Earth's atmosphere: Proceedings of the National Academy of Sciences of the United States of America, v. 110, n. 42, p. 16736–16741, https://doi.org/10.1073/pnas.1315570110

Canfield, D. E., Zhang, S., Wang, H., Wang, X., Zhao, W., Su, J., Bjerrum, C. J., Haxen, E. R., and Hammarlund, E. U., 2018, A Mesoproterozoic iron formation: Proceedings of the National Academy of Sciences, v. 115, n. 17, https://doi.org/10.1073/pnas.1720529115

Canfield, D. E., Knoll, A. H., Poulton, S. W., Narbonne, G. M., and Dunning, G. R., 2020, Carbon isotopes in clastic rocks and the Neoproterozoic carbon cycle: American Journal of Science, v. 320, n. 2, p. 97–124, https://doi.org/10.2475/02.2020.01

Cawood, P. A., Hawkesworth, C., and Dhuime, B., 2013, The continental record and the generation of continental crust: Geological Society of America Bulletin, v. 125, n. p. 1–2.14p. –32, https://doi.org/10.1130/B30722.1

Chang, S., and Berner, R. A., 1999, Coal weathering and the geochemical carbon cycle: Geochimica et Cosmochimica Acta, v. 63, n. 19–20, p. 3301–3310, https://doi.org/10.1016/S0016-7037(99)00252-5

Clayton, J. L., and Bostick, N. H., 1986, Temperature effects on kerogen and on molecular and isotopic composition of organic matter in Pierre Shale near an igneous dike: Organic Geochemistry, v. 10 n. 1–3, p. 135–143, https://doi.org/10.1016/0146-6380(86)90017-3

Cloud, P. E., Jr., 1972, A working model of the primitive Earth: American Journal of Science, v. 272, n. 6, p. 537–548, https://doi.org/10.2475/ajs.272.6.537

Condie, K. C., Des, M. D. J., and Abbott, D., 2001, Precambrian superplumes and supercontinents: A record in black shales, carbon isotopes, and paleoclimates?: Precambrian Research, v. 106, n. 3–4, p. 239–260, https://doi.org/10.1016/S0301-9268(00)00097-8

Crockford, P. W., Kunzmann, M., Bekker, A., Hayles, J., Bao, H., Halverson, G. P., Peng, Y., Bui, T. H., Cox, G. M., Gibson, T. M., Wörndle, S., Rainbird, R., Lepland, A., Swanson-Hysell, N. L., Master, S., Sreenivas, B., Kuznetsov, V., and Krupenik, V., and Wing, B. A., 2019, Claypool continued: Extending the isotopic record of sedimentary sulfate: Chemical Geology, v. 513, p. 200–225, https://doi.org/10.1016/j.chemgeo.2019.02.030

Crowe, S. A., Dossing, L. N., Beukes, N. J., Bau, M., Kruger, S. J., Frei, R., and Canfield, D. E., 2013, Atmospheric oxygenation three billion years ago: Nature, v. 501, p. 535–538, https://doi.org/10.1038/nature12426

Daines, S. J., Mills, B. J. W., and Lenton, T. M., 2017, Atmospheric oxygen regulation at low Proterozoic levels by incomplete oxidative weathering of sedimentary organic carbon: Nature Communications, v. 8, p. 14379, https://doi.org/10.1038/ncomms14379

Deines, P., 1980, The carbon isotopic composition of diamonds: Relationship to diamond shape, color, occurrence and vapor composition: Geochimica et Cosmochimica Acta, v. 44, n. 7, p. 943–961, https://doi.org/10.1016/0016-7037(80)90284-7

DeLucia, M. S., Guenthner, W. R., Marshak, S., Thomson, S. N., and Ault, A. K., 2017, Thermochronology links denudation of the Great Unconformity surface to the supercontinent cycle and snowball Earth: Geology, v. 46, n. 2, p. 167–170, https://doi.org/10.1130/G39525.1

Des Marais, D. J., Strauss, H., Summons, R. E., and Hayes, J. M., 1992, Carbon isotope evidence for the stepwise oxidation of the Proterozoic environment: Nature, v. 359, p. 605–609, https://doi.org/10.1038/359605a0

Dhuime, B., Hawkesworth, C. J., Cawood, P. A., and Storey, C. D., 2012, A change in the geodynamics of continental growth 3 billion years ago: Science (New York, N.Y.), v. 335, n. 6074, p. 1334–1336, https://doi.org/10.1126/science.1216066

Dickens, A. F., Gélinas, Y., and Hedges, J. I., 2004a, Physical separation of combustion and rock sources of graphitic black carbon in sediments: Marine Chemistry, v. 92, n. 1–4, p. 215–223, https://doi.org/10.1016/j.marchem.2004.06.027

Dickens, A. F., Gélinas, Y., Masiello, C. A., Wakeham, S., and Hedges, J. I., 2004b, Reburial of fossil organic carbon in marine sediments: Nature, v. 427, p. 336–339, https://doi.org/10.1038/nature02299

Fakhraee, M., Planavsky, N. J., and Reinhard, C. T., 2020, The role of environmental factors in the long-term evolution of the marine biological pump: Nature Geoscience, v. 13, p. 812–816, https://doi.org/10.1038/s41561-020-00660-6

Farquhar, J., Bao, H. M., and Thiemens, M., 2000, Atmospheric influence of Earth's earliest sulfur cycle: Science (New York, N.Y.), v. 289, n. 5480, p. 756–758, https://doi.org/10.1126/science.289.5480.756

Farquhar, J., Peters, M., Johnston, D. T., Strauss, H., Masterson, A., Wiechert, U., and Kaufman, A. J., 2007, Isotopic evidence for Mesoarchaean anoxia and changing atmospheric sulphur chemistry: Nature, v. 449, p. 706–709, https://doi.org/10.1038/nature06202

Fischer, W. W., Schroeder, S., Lacassie, J. P., Beukes, N. J., Goldberg, T., Strauss, H., Horstmann, U. E., Schrag, D. P., and Knoll, A. H., 2009, Isotopic constraints on the Late Archean carbon cycle from the Transvaal Supergroup along the western margin of the Kaapvaal Craton, South Africa: Precambrian Research, v. 169, n. 1–4, p. 15–27, https://doi.org/10.1016/j.precamres.2008.10.010

Galy, V., Beyssac, O., France-Lanord, C., and Eglinton, T., 2008, Recycling of graphite during Himalayan erosion: A geological stabilization of carbon in the crust: Science (New York, N.Y.), v. 322, n. 5903, p. 943–945, https://doi.org/10.1126/science.1161408

Galy, V., Peucker-Ehrenbrink, B., and Eglinton, T., 2015, Global carbon export from the terrestrial biosphere controlled by erosion: Nature, v. 521, p. 204–207, https://doi.org/10.1038/nature14400

Geyman, E. C., and Maloof, A. C., 2019, A diurnal carbon engine explains ^{13}C-enriched carbonates without increasing the global production of oxygen: Proceedings of the National Academy of Sciences of the United States of America, v. 116, n. 49, p. 24433–24439, https://doi.org/10.1073/pnas.1908783116

González-Álvarez, I., and Kerrich, R., 2012, Weathering intensity in the Mesoproterozoic and modern large-river systems: A comparative study in the Belt-Purcell Supergroup: Precambrian Research, v. 208, p. 174–196, https://doi.org/10.1016/j.precamres.2012.04.008

Haberstroh, P. R., Brandes, J. A., Gélinas, Y., Dickens, A. F., Wirick, S., and Cody, G., 2006, Chemical composition of the graphitic black carbon fraction in riverine and marine sediments at sub-micron scales using carbon X-ray spectromicroscopy: Geochimica et Cosmochimica Acta, v. 70, n. 6, p. 1483–1494, https://doi.org/10.1016/j.gca.2005.12.001

Halverson, G. P., Hoffman, P. F., Schrag, D. P., Maloof, A. C., and Rice, A. H. N., 2005, Toward a Neoproterozoic composite carbon isotope record: GSA: Geological Society of America Bulletin, v. 117 n. 9–10, p. 1181–1207, https://doi.org/10.1130/B25630.1

Hao, J., Knoll, A. H., Huang, F., Schieber, J., Hazen, R. M., and Daniel, I., 2020, Cycling phosphorus on the Archean Earth: Part II. Phosphorus limitation on primary production in Archean ecosystems: Geochemica : Geochimica et Cosmochimica Acta, v. 280, p. 360–377, https://doi.org/10.1016/j.gca.2020.04.005

Hardisty, D. S., Lu, Z. L., Planavsky, N. J., Bekker, A., Philippot, P., Zhou, X. L., and Lyons, T. W., 2014, An iodine record of Paleoproterozoic surface ocean oxygenation: Geology, v. 42, n. 7, p. 619–622, https://doi.org/10.1130/G35439.1

Harrison, T. M. , 2020, Hadean Earth: Cham, Switzerland, Springer, p. 291

Hay, W. W., Sloan, I. I. J. L., and Wold, C. N., 1988, Mass/age distribution and composition of sediments on the ocean floor and the global rate of sediment subduction: Journal of Geophysical Research: Solid Earth, v. 12, p. 14933–14940, https://doi.org/10.1029/JB093iB12p14933

Hayes, J. M., and Waldbauer, J. R., 2006, The carbon cycle and associated redox processes through time: Philosophical transactions of the Royal Society of Londo n. Series B, Biological Sciences, p. 931–950, https://doi.org/10.1098/rstb.2006.1840

Hayes, J. M., Strauss, H., and Kaufman, A. J., 1999, The abundance of ^{13}C in marine organic matter and isotopic fractionation in the global biogeochemical cycle of carbon during the past 800 Ma: Chemical Geology: Chemical Geology, v. 161, n. 1–3, p. 103–125, https://doi.org/10.1016/S0009-2541(99)00083-2

Herman, F., Seward, D., Valla, P. G., Carter, A., Kohn, B., Willett, S. D., and Ehlers, T. A., 2013, Worldwide acceleration of mountain erosion under a cooling climate: Nature, v. 504, p. 423–426, https://doi.org/10.1038/nature12877

Hilting, A. K., Kump, L. R., and Bralower, T. J., 2008, Variations in the oceanic vertical carbon isotope gradient and their implications for the Paleocene-Eocene biological pump: Paleoceanography and Paleoceanography, v. 23, n. 3, https://doi.org/10.1029/2007PA001458

Hoffman, P. F., and Lamothe, K. G., 2019, Seawater-buffered diagenesis, destruction of carbon isotope excursions, and the composition of DIC in Neoproterozoic oceans: Proceedings of the National Academy of Sciences of the United States of America, v. 116, n. 38, p. 18874–18879, https://doi.org/10.1073/pnas.1909570116

Holland, H. D. (1978).The Chemistry of the Atmosphere and Oceans: New York, John Wiley and Sons, p. 351

——(1994).Early Proterozoic atmospheric change , in Bengston, S., editor, Early Life on Earth: New York, Columbia University Press, p. 237–244.

Holland, H. D., 1999, When did the Earth's atmosphere become oxic? : A reply: The Geochemical News, v. 100, p. 20–22.

Holser, W. T., Schidlowski, M., Mackenzie, F. T., and Maynard, J. B., 1988, Geochemical cycles of carbon and sulfur , in Gregor, C. B., Garrels, R. M., M., F. T., and Maynard, J. B. editors, Chemical Cycles in the Evolution of the Earth: New York, John Wiley and Sons, p. 105–173.

Husson, J. M., and Peters, S. E., 2017, Atmospheric oxygenation driven by unsteady growth of the continental sedimentary reservoir: Earth and Planetary Science Letters, v. 460, p. 68–75, https://doi.org/10.1016/j.epsl.2016.12.012

James, H. L. (1983).Distribution of banded iron-formation in space and time, *in* Trendall, A. F., and Morris, R. C., editors, Iron-formation: Facts and Problems: Amsterdam, Elseviers Science Publishers B. V., Developments in Precambrian Geology, v. 6, p. 471–490,

Johnson, A. C., Romaniello, S. J., Reinhard, C. T., Gregory, D. D., Garcia-Robledo, E., Revsbech, N. P., Canfield, D. E., Lyons, T. W., and Anbar, A. D., 2019, Experimental determination of pyrite and molybdenite oxidation kinetics at nanomolar oxygen concentrations: Geochimica et Cosmochimica Acta, v. 249, p. 160–172, https://doi.org/10.1016/j.gca.2019.01.022

Karhu, J. A., and Holland, H. D., 1996, Carbon isotopes and the rise of atmospheric oxygen: Geology, v. 24, n. 10, p. 867–870., https://doi.org/10.1130/0091-7613(1996)024<0867:CIATRO>2.3.CO;2

Kasting, J. F., Zahnle, K. J., and Walker, J. C. G., 1983, Photochemistry of methane in the Earth's early atmosphere: Precambrian Research, v. 20, n. 2–4, p. 121–148, https://doi.org/10.1016/0301-9268(83)90069-4

Kirschvink, J. L., and Kopp, R. E., 2008, Palaeoproterozoic ice houses and the evolution of oxygen-mediating enzymes: The case for a late origin of photosystem II: Philosophical Transactions of the Royal Society B: Biological Sciences, v. 363, n. 1504, p. 2755–2765, https://doi.org/10.1098/rstb.2008.0024

Konhauser, K. O., Hamade, T., Raiswell, R., Morris, R. C., Ferris, F. G., Southam, G., and Canfield, D. E., 2002, Could bacteria have formed the Precambrian banded iron formations?: Geology, v. 30, n. 12, p. 1079–1082., https://doi.org/10.1130/0091-7613(2002)030<1079:CBHFTP>2.0.CO;2

Konhauser, K. O., Planavsky, N. J., Hardisty, D. S., Robbins, L. J., Warchola, T. J., Haugaard, R., Lalonde, S. V., Partin, C. A., Oonk, P. B. H., Tsikos, H., Lyons, T. W., Bekker, A., and Johnson, C. M., 2017, Iron formations: A global record of Neoarchaean to Paleoproterozoic environmental history: Earth-Science Reviews, v. 172, p. 140–177, https://doi.org/10.1016/j.earscirev.2017.06.012

Korenaga, J., 2018, Estimating the formation age distribution of continental crust by unmixing zircon ages: Earth and Planetary Science Letters, v. 482, p. 388–395, https://doi.org/10.1016/j.epsl.2017.11.039

Krissansen-Totton, J., Buick, R., and Catling, D. C., 2015, A statistical analysis of the carbon isotope record from the Archean to Phanerozoic and implications for the rise of oxygen: American Journal of Science, p. 275–316, https://doi.org/10.2475/04.2015.01

Lajoinie, M. F., Lanfranchini, M. E., Recio, C., Sial, A. N., Cingolani, C. A., Ballivián Justiniano, C. B., and Etcheverry, R. O., 2019, The Lomagundi-Jatuli carbon isotopic event recorded in the marble of the Tandilia System basement, Río de la Plata Craton, Argentina: Precambrian Research, v. 326, p. 447–461, https://doi.org/10.1016/j.precamres.2018.03.012

Li, Z., Peterse, F., Wu, Y., Bao, H., Eglinton, T. I., and Zhang, J., 2015, Sources of organic matter in Changjiang (Yangtze River) bed sediments: Preliminary insights from organic geochemical proxies: Organic Geochemistry, v. 85, p. 11–21, https://doi.org/10.1016/j.orggeochem.2015.04.006

Logan, G. A., Hayes, J. M., Hieshima, G. B., and Summons, R. E., 1995, Terminal Proterozoic reorganization of biogeochemical cycles: Nature, v. 376, p. 53–56, https://doi.org/10.1038/376053a0

Lohmann, K. C., 1988, Goechemical patterns of meteoric diagenetic systems and their application to studies of paleokarst, *in* James, N. P., and Choquette, P. W., editors, Paleokarst: New York, Springer-Verlag New York, Inc., p. 58–80,

Laakso, T. A., and Schrag, D. P., 2019, A small marine biosphere in the Proterozoic: Geobiology, v. 17, n. 2, p. 161–171, https://doi.org/10.1111/gbi.12323

Mackenzie, F. T., and Morse, J. W., 1992, Sedimentary carbonates through Phanerozoic time: Geochimica et Cosmochimica Acta, v. 56, p. 3281–3295, https://doi.org/10.1016/0016-7037(92)90305-3

Magnabosco, C., Moore, K. R., Wolfe, J. M., and Fournier, G. P., 2018, Dating phototrophic microbial lineages with reticulate gene histories: Geobiology, v. 16, n. 2, p. 179–189, https://doi.org/10.1111/gbi.12273

Maheshwari, A., Sial, A. N., Gaucher, C., Bossi, J., Bekker, A., Ferreira, V. P., and Romano, A. W., 2010, Global nature of the Paleoproterozoic Lomagundi carbon isotope excursion: A review of occurrences in Brazil, India, and Uruguay: Precambrian Research, p. 274–299, https://doi.org/10.1016/j.precamres.2010.06.017

Martin, W. F., Bryant, D. A., and Beatty, J. T., 2018, A physiological perspective on the origin and evolution of photosynthesis: FEMS Microbiology Reviews, v. 42, n. 2, p. 205–231, https://doi.org/10.1093/femsre/fux056

Mason, E., Edmonds, M., and Turchyn, A. V., 2017, Remobilization of crustal carbon may dominate volcanic arc emissions: Science (New York, N.Y.), v. 357, n. 6348, p. 290–294, https://doi.org/10.1126/science.aan5049

McLennan, S. M., 1988, Recycling of the continental crust: Pure and Applied Geophysics Pageoph, v. 128, p. 683–724, https://doi.org/10.1007/BF00874553

Melezhik, V. A., Fallick, A. E., Filippov, M. M., and Larsen, O., 1999a, Karelian shungite-an indication of 2.0-Ga-old metamorphosed oil-shale and generation of petroleum: Geology, lithology and geochemistry: Earth-Science Reviews, : v. 47, n. 1–2, p. 1, –40, https://doi.org/10.1016/S0012-8252(99)00027-6

Melezhik, V. A., Fallick, A. E., Medvedev, P. V., and Makarikhin, V. V., 1999b, Extreme $^{13}C_{carb}$ enrichment in *ca*. 2.0 Ga magnesite-stromatolite-dolomite-"red beds" association in a global context: A case for the world-wide signal enhanced by a local environment: Earth-Science Reviews, v. 48, n. 1–2, p. 71–120, https://doi.org/10.1016/S0012-8252(99)00044-6

Melezhik, V. A., Filippov, M. M., and Romashkin, A. E., 2004, A giant Palaeoproterozoic deposit of shungite in NW Russia: Genesis and practical applications: Ore Geology Reviews, v. 24n1, –2, p. 135–154, https://doi.org/10.1016/j.oregeorev.2003.08.003

Melezhik, V. A., Fallick, A. E., Hanski, E. J., Kump, L. R., Lepland, A., Prave, A. R., and Strauss, H., 2005, Emergence of the aerobic biosphere during the Archean-Proterozoic transition: Challenges of future research: GSA Today, v. 15, n, 11, p. 4–11., https://doi.org/10.1130/1052-5173(2005)015[4:EOAABD]2.0.CO;2

Milliman, J. D., and Farnsworth, K. L., 2013, River discharge to the coastal ocean: A global synthesis: Cambridge, England, Cambridge University Press, 394 p., https://doi.org/10.1017/CBO 9780511781247

Miyazaki, Y., Planavsky, N. J., Bolton, E. W., and Reinhard, C. T., 2018, Making sense of massive carbon isotope excursions with an inverse carbon cycle model: Journal of Geophysical Research: Biogeosciences, v. 123, n. 8, p. 2485–2496, https://doi.org/10.1029/2018JG004416

Mojzsis, S. J., Harrison, T. M., and Pidgeon, R. T., 2001, Oxygen-isotope evidence from ancient zircons for liquid water at the Earth's surface 4,300 Myr ago: Nature, v. 409, p. 178–181, https://doi.org/10.1038/35051557

Partin, C. A., Bekker, A., Planavsky, N. J., Scott, C. T., Gill, B. C., Li, C., Podkovyrov, V., Maslov, A., Konhauser, K. O., Lalonde, S. V., Love, G. D., Poulton, S. W., and Lyons, T. W., 2013, Large-scale fluctuations in Precambrian atmospheric and oceanic oxygen levels from the record of U in shales: Earth and Planetary Science Letters, v. 369–370, p. 284–293, https://doi.org/10.1016/j.epsl.2013.03.031

Pavlov, A. A., and Kasting, J. F., 2002, Mass-independent fractionation of sulfur isotopes in Archean sediments: Strong evidence for an anoxic Archean atmosphere: Astrobiology, v. 2, n. 1, p. 27–41, https://doi.org/10.1089/153110702753621321

Petsch, S., 2014, Weathering of organic carbon : Treatise on Geochemistry (second edition), v. 12, p. 217–238, https://doi.org/10.1016/B978-0-08-095975-7.01013-5

Petsch, S. T., Berner, R. A., and Eglinton, T. I., 2000, A field study of the chemical weathering of ancient sedimentary organic matter: Organic Geochemistry, v. 31, n. 5, p. 475–487, https://doi.org/10.1016/S0146-6380(00)00014-0

Raiswell, R., and Berner, R. A., 1987, Organic carbon losses during burial and thermal maturation of normal marine shales: Geology, v. 15, n. 9, p. 853–857., https://doi.org/10.1130/0091-7613(1987)15<853:OCLDBA>2.0.CO;2

Ronov, A. B., 1976, Global carbon geochemistry, volcanism, carbonate accumulation, and life: Translated from Geokhimiya, v, v. 8, p. 1252–1277.

Ronov, A. B., Khain, V. E., Balukhovsky, A. N., and Seslavinsky, K. K., 1980, Quantitative analysis of Phanerozoic sedimentation: Sedimentary Geology: Sedimentary Geology, p. 311–325, https://doi.org/10.1016/0037-0738(80)90067-6

Rosas, J. C., and Korenaga, J., 2018, Rapid crustal growth and efficient crustal recycling in the early Earth: Implications for Hadean and Archean geodynamics: Earth and Planetary Science Letters, v. 494, p. 42–49, https://doi.org/10.1016/j.epsl.2018.04.051

Rosing, M. T., 1999, ^{13}C-depleted carbon microparticles in >3700-Ma sea-floor sedimentary rocks from West Greenland: Science (New York, N.Y.), v. 283, n. 5402, p. 674–676, https://doi.org/10.1126/science.283.5402.674

Saltzman, M. R., and Thomas, E., 2012, Carbon isotope stratigraphy: The Geologic Time Scale, p. 207–232, https://doi.org/10.1016/B978-0-444-59425-9.00011-1

Sánchez-García, L., de Andrés, J. R., Gélinas, Y., Schmidt, M. W. I., and Louchouarn, P., 2013, Different pools of black carbon in sediments from the Gulf of Cádiz (SW Spain): Method comparison and spatial distribution: Marine Chemistry, v. 151, p. 13–22, https://doi.org/10.1016/j.marchem.2013.02.006

Schidlowski, M., Hayes, J. M., and Kaplan, I. R. (1983).Isotopic inferences of ancient biogeochemistries: carbon, sulfur, hydrogen, and nitrogen , in Schopf, J. W., editor, Earth's Earliest Biosphere: It's Origin and Evolution: Princeton, New Jersey, Princeton University Press, p. 149–186.

Schrag, D. P., Higgins, J. A., Macdonald, F. A., and Johnston, D. T., 2013, Authigenic carbonate and the history of the global carbon cycle: Science (New York, N.Y.), v. 339, n. 6119, p. 540–543, https://doi.org/10.1126/science.1229578

Schröder, S., Bekker, A., Beukes, N. J., Strauss, H., and Van Niekerk, H. S., 2008, Rise in seawater sulphate concentration associated with the Paleoproterozoic positive carbon isotope excursion: Evidence from sulphate evaporites in the ~2.2–2.1 Gyr shallow-marine Lucknow Formation, South Africa: Terra Nova, v. 20, n. 2, p. 108–117, https://doi.org/10.1111/j.1365-3121.2008.00795.x

Shih, P. M., Hemp, J., Ward, L. M., Matzke, N. J., and Fischer, W. W., 2017, Crown group Oxyphotobacteria postdate the rise of oxygen: Geobiology, v. 15, n. 1, p. 19–29, https://doi.org/10.1111/gbi.12200

Sleep, N. H., and Zahnle, K., 2001, Carbon dioxide cycling and implications for climate on ancient: Journal of Geophysical Research: Planets, p. 1373–1399, https://doi.org/10.1029/2000JE001247

Southam, J. R., and Hay, W. W., 1981, Global sedimentary mass balance and sea level changes, *in* Emiliani, C., editor: The Sea: New York, Wiley, The Oceanic Lithosphere, v. 7, p. 1617–1683.

Sparkes, R. B., Hovius, N., Galy, A., and Liu, J. T., 2020, Survival of graphitized petrogenic organic carbon through multiple erosional cycles: Earth and Planetary Science Letters, v. 531, p. 115992, https://doi.org/10.1016/j.epsl.2019.115992

Swart, P. K., 2015, The geochemistry of carbonate diagenesis: The past, present and future: Sedimentology, v. 62, n. 5, p. 1233–1304, https://doi.org/10.1111/sed.12205

Tice, M. M., and Lowe, D. R., 2004, Photosynthetic microbial mats in the 3,416-Myr-old ocean: Nature, v. 431, p. 549–552, https://doi.org/10.1038/nature02888

——2006a, Hydrogen-based carbon fixation in the earliest known photosynthetic organisms: Geology, v. 34, n. 1, p. 37–40, https://doi.org/10.1130/G22012.1

——2006b, The origin of carbonaceous matter in pre-3.0 Ga greenstone terrains: A review and new evidence from the 3.42 Ga Buck Reef Chert: Earth-Science Reviews, v. 76, n. 3–4, p. 259–300, https://doi.org/10.1016/j.earscirev.2006.03.003

Tissot, B. P., and Welte, D. H. (1984).Petroleum formation and occurrence: New York, Springer-Verlag, p. 702

Ueno, Y., Yoshioka, H., Maruyama, S., and Isozaki, Y., 2004, Carbon isotopes and petrography of kerogens in~ 3.5-Ga hydrothermal silica dikes in the North Pole area, Western Australia: Geochimica et Cosmochimica Acta, v. 68, n. 3, p. 573–589, https://doi.org/10.1016/S0016-7037(03)00462-9

Ueno, Y., Yamada, K., Yoshida, N., Maruyama, S., and Isozaki, Y., 2006, Evidence from fluid inclusions for microbial methanogenesis in the early Archaean era: Nature, v. 440, p. 516–519, https://doi.org/10.1038/nature04584

Veizer, J., and Jansen, S. L., 1985, Basement and sedimentary recycling-2: Time dimension to global tectonics: The Journal of Geology, v. 93, n. 6, p. 625–643, https://doi.org/10.1086/628992

Ward, L. M., and Shih, P. M., 2019, The evolution and productivity of carbon fixation pathways in response to changes in oxygen concentration over geological time: Free Radical Biology and Medicine, v. 140, p. 188–199, https://doi.org/10.1016/j.freeradbiomed.2019.01.049

Ward, L. M., Kirschvink, J. L., and Fischer, W. W., 2016, Timescales of Oxygenation following the evolution of oxygenic photosynthesis: Origins of Life and Evolution of the Biosphere: The Journal of the International Society for the Study of the Origin of Life, v. 46, p. 51–65, https://doi.org/10.1007/s11084-015-9460-3

Warke, M. R., Di Rocco, T., Zerkle, A. L., Lepland, A., Prave, A. R., Martin, A. P., Ueno, Y., Condon, D. J., and Claire, M. W., 2020, The Great Oxidation Event preceded a Paleoproterozoic: Proceedings of the National Academy of Sciences of the United States of America, Snowball Earth, v. 117, n. 24, p. 13314–13320, https://doi.org/10.1073/pnas.2003090117

Wilde, S. A., Valley, J. W., Peck, W. H., and Graham, C. M., 2001, Evidence from detrital zircons for the existence of continental crust and oceans on the Earth 4.4 Gyr ago: Nature, v. 409, p. 175–178, https://doi.org/10.1038/35051550

Wilkinson, B. H., and Walker, J. C. G., 1989, Phanerozoic cycling of sedimentary carbonate: American Journal of Science, v. 289, n. 4, p. 525–548, https://doi.org/10.2475/ajs.289.4.525

Wille, M., Kramers, J. D., Nagler, T. F., Beukes, N. J., Schroder, S., Meisel, T., Lacassie, J. P., and Voegelin, A. R., 2007, Evidence for a gradual rise of oxygen between 2.6 and 2.5 Ga from Mo isotopes and Re-PGE signatures in shales: Geochimica et Cosmochimica Acta, v. 71, n. 10, p. 2417–2435, https://doi.org/10.1016/j.gca.2007.02.019

Wittmann, H., Oelze, M., Gaillardet, J., Garzanti, E., and von Blanckenburg, F., 2020, A global rate of denudation from cosmogenic nuclides in the Earth's largest rivers: Earth-Science Reviews, v. 204, p. 103147, https://doi.org/10.1016/j.earscirev.2020.103147

Zahnle, K., Claire, M., and Catling, D., 2006, The loss of mass-independent fractionation in sulfur due to a Palaeoproterozoic collapse of atmospheric methane: Geobiology, v. 4, n. 4, p. 271–283, https://doi.org/10.1111/j.1472-4669.2006.00085.x

Zhang, S. C., Wang, X. M., Wang, H. J., Bjerrum, C. J., Hammarlund, E. U., Costa, M. M., Connelly, J. N., Zhang, B. M., Su, J., and Canfield, D. E., 2016, Sufficient oxygen for animal respiration 1,400 million years ago: Proceedings of the National Academy of Sciences, v. 113, n. 7, p. 1731–1736, https://doi.org/10.1073/pnas.1523449113